NIST Technical Note 1835

Nanoparticle Released from Consumer Products: Flooring Nanocoatings and Interior Nanopaints

Final Report to U.S. Consumer Product Safety Commission Interagency Agreement CPSC-I-12-0007

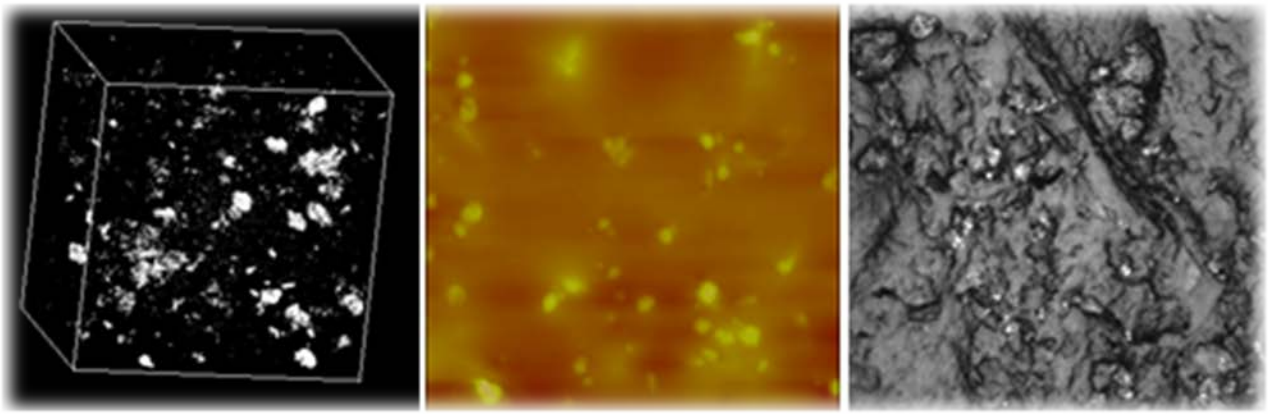

Lipiin Sung
Tinh Nguyen
Andrew Persily

http://dx.doi.org/10.6028/NIST.TN.1835
July 15, 2014

National Institute of Standards and Technology
U.S. Department of Commerce

NIST Technical Note 1835

Nanoparticle Released from Consumer Products: Flooring Nanocoatings and Interior Nanopaints

Final Report to U.S. Consumer Product Safety Commission Interagency Agreement CPSC-I-12-0007

Lipiin Sung
Tinh Nguyen

Materials and Structural Systems Division
Engineering Laboratory

Andrew Persily

Energy and Environment Division
Engineering Laboratory

http://dx.doi.org/10.6028/NIST.TN.1835

July 2014

U.S. Department of Commerce
Rebecca Blank, Acting Secretary

National Institute of Standards and Technology
Patrick D. Gallagher, Under Secretary of Commerce for Standards and Technology and Director

National Institute of Standards and Technology Technical Note 1835
Natl. Inst. Stand. Technol. Tech. Note 1835, 68 pages (July 2014)
http://dx.doi.org/10.6028/NIST.TN.1835
CODEN: NTNOEF

Table of Contents

ABSTRACT

Nanoparticles are increasingly incorporated in flooring coatings and interior paints to improve their abrasion and microbial resistance. One particular concern of this application is the release of nanoparticles from these surfaces due to repeated mechanical forces acted upon them, such as walking, mopping, cleaning, scratching, and furniture moving. Such release of the nanosize material is potentially harmful to the occupants, particularly children who typically experience greater exposure to substances deposited at floor level. Because of these concerns, Consumer Product Safety Commission (CPSC) and National Institute of Standards and Technology (NIST) entered into an agreement to develop testing and measurement protocols for determining the quantities and properties of nanoparticles released from flooring coatings and interior paints. The first year of this research was devoted to developing instrumentation, protocols, and analytical methods to measure released particles during abrasion in air (dry conditions) from flooring coatings and interior paints containing a known amount of nanoparticles. The second year of the research has investigated the development of methods and protocols for abrasion of flooring coatings and interior paints and to measure and identify the particles remaining on the surface and in liquid. This report summarizes the Year 2 research, which studied a nanocoating used on commercial flooring and an interior nanopaint, including: 1) characterization of inorganic materials in the commercial nanoproducts and initial properties before and after immersion in water, 2) development of methods and protocols for abrasion in liquid of the flooring nanocoating and interior nanopaint, 3) measurement and identification of released particles remaining on the abraded surfaces and suspended in liquid, and 4) development of an abrasion wheel that can reproducibly abrade nanocoating and nanopaint surfaces in air and in liquid.

LIST OF FIGURES

LIST OF TABLES

1. Introduction

Polymeric nanocomposites refer to multicomponent systems in which the major constituent is a polymer or its blends and the minor constituent is a filler having at least one dimension below 100 nm (e.g., spherical nanoparticles, layered platelets, tubes, or rods). Polymeric nanocomposites differ from traditional filled plastics or fiber-reinforced composites in that they provide greatly enhanced properties, such as mechanical enhancement, gas barrier, and flame retardancy, with minimum effects on mass and processing modifications. For that reason, these advanced composite materials have been an area of intense industrial and academic research for the past two decades, as strongly evidenced in recent extensive reviews on polymer nanocomposites for a variety of nanofillers [1-5]. Due to the enormous potential of nanotechnology, many companies across the world are investing heavily in this sector. In 2006, about 300 commercial products on the market claimed to contain nanomaterials made by a few companies [6]. In 2013, more than 1300 manufacturers have nano-enabled products in the commercial market, with a value of 1.6 trillion US dollars and an annual growth of more than 49 % between 2009 to 2013 [7]. In the past few years, polymer nanocomposite applications have gained a strong commercial footing, due to the outstanding performance of these advanced materials and the efforts of resin manufacturers and compounders who offer easy-to-process and nanoparticle-compatible products [8]. Although applications vary widely, polymer nanocomposites generally take advantage of exceptional nanofiller properties. Depending on the types of nanofillers used, advantages of polymer nancomposites over traditional polymer products include their being stronger, harder, tougher, lighter, more stable, less permeable, and more durable.

In coming years, polymer nanocomposites will likely enter the consumer markets in large quantities in consumer products and in large-volume industries such as textiles, construction, automotive, etc. Regardless of the application, both the long-term performance of the polymer nanocomposite itself and the fate of the nanofillers in the matrix during the product's life cycle play a key role in the commercialization and uses of these nanocomposite products. The main reason for that is nanofillers that were embedded in the polymer matrices may be released from the nanocomposites during their life cycle. Another reason is most commercial polymers are susceptible to attack by the environments (i.e., deterioration or aging),

which result in an increase in brittleness, loss of mechanical properties, and cracking of the nanocomposites. The consequence of this matrix deterioration is promoting the migration and release of nanofillers from the nanocomposites. Because nanosize materials have shown potential risks to the environment, health and safety (EHS) [9-15], the latent release of the nanofillers during the life cycle of a polymer nanocomposite would present a roadblock to widespread uses of these advanced composites.

Several recent studies have presented various possible accidental and incidental scenarios of nanomaterial release during the life cycle of nanocomposites used in a variety of industries including construction, textiles, tires, and consumer products [15-19]. In general, the release of nanomaterials from the polymer nanocomposites occurs not only during production of the nanocomposites, but also during their use, recycling, disposal, and incineration. The prevailing release routes may be different for different applications. For consumer products, such as sporting goods, electronics, and flooring coatings, mechanical forces, recycling, and incineration of solid wastes could be the main release routes. For textiles, in addition to release by mechanical and matrix degradation mechanisms and their synergistic effects, recycled textiles undergo various mechanical, thermal and chemical treatments that could also release nanomaterials from the composite fibers. Although the extent of release may be different at different stages of their respective life cycle, these scenarios should be generally applicable to other industries, such as construction, tires, consumer products, and automobiles. As such, it can be expected that some fraction of nanomaterials that has been incorporated in the polymer matrix will be eventually released into the environment during a product's life cycle. Further, in addition to release, these various mechanisms could also expose nanomaterials on the nanocomposite surface. Despite the serious potential risks posed by surface accumulation and release of nanofillers during the life cycle of polymer nanocomposites, little data is available about the fate of embedded nanofillers in the nanocomposites, how they may be released, and the quantity, composition, and structure of the released particles throughout the product's life cycle. This lack of information hinders our ability to understand the release mechanisms, to predict the release rates, to quantify human exposure, and to develop strategies for mitigating this potential hazard. Therefore, the long term performance and the potentially harmful effects of the nanofillers incorporated in polymer matrices on the EHS cannot be determined.

One particularly large industry segment that increasingly incorporates nanomaterials in their products is polymeric coatings, which are commonly used to protect, enhance, or decorate wood, plastic and metal products used in homes and other buildings. The coating nanotechnology segment is projected to increase from $3.4 billion in 2010 to nearly $18 billion in 2015, an average annual increase of 39.5 % [20]. The main markets for nanocoatings are currently focused on easy-cleaning, self-cleaning, dirt resistant, impermeable, and scratch-resistant products. However, because polymeric materials are generally mechanically weak, the coatings and the surfaces to which they are applied are susceptible to scratching, abrasion, and chipping during manufacture, shipping, and use. Metal oxide nanoparticles, such as alumina (Al_2O_3), titania (TiO_2) and nonmetal oxides, such as silicon dioxide (SiO_2), are increasingly being added to coating formulations to significantly reduce or prevent such damage as well as to enhance properties such as microbial and mildew resistance [1]. These metal oxide nanoparticles serve many functions in the coatings industry. Alumina and silicon dioxide nanoparticles are used to enhance the mechanical and scratch resistance of coatings. TiO_2 and ZnO are traditionally used as pigments to enhance the appearance and improve the durability of polymeric products. However, due to their ability to absorb broad band ultraviolet (UV), these materials at nanosize have been exploited in self-cleaning coatings, UV-resistant coatings, sunscreens, and disinfectant sprays. These nanomaterials are also used for modifying optical properties, for example, increasing the refractive index of coatings. Due to their aid in surface cleaning, TiO_2 nanoparticles are currently used in interior paints for kitchens and bathrooms. A variety of commercial coatings and paints containing nanoparticles from a number of companies are widely available to consumers.

Research in the past few years on the health effects of nanomaterials has focused mainly on human and environmental exposure during manufacturing. However, the release of these nanoparticles from products of high volume industries such as flooring coatings (finishes), interior paints, and other consumer products over their service life, and the resulting exposure of building occupants to particles deposited on building surfaces, potentially poses risks similar to those encountered during manufacturing. This is because 1) the population of general building occupants is much greater than those involved only in manufacturing; 2) the amount of surface area of interior walls and floorings in residential and commercial buildings is very large, and 3) the human exposure to these nanoparticles may be continuous over the entire service life of the

products. Flooring coatings are of particular concern for young children who spend more time on the floor and, therefore, have greater opportunities for exposure. Despite these potential risks, little information is available on the in-service release, surface accumulation, transport, and exposure to nanoparticles from flooring coatings and interior paints. Lack of such data severely hinders the ability to quantitatively assess and manage the potential health effects of nanoparticle release from these large-volume sources.

For flooring coatings and interior paints, the main mechanism of nanofiller release is by mechanical forces, such as abrasion, polishing, sanding, and mopping. Release by mechanical mechanisms has been investigated by a number of researchers for coatings containing multiwall carbon nanotubes (MWCNTs) [19, 21, 22], ZnO, Fe_2O_3 [23,24], TiO_2 [25,26], SiO_2 [19,26], and clay [27] nanoparticles. Taber abrasers, linear or rotary, are often utilized in these studies to generate particles for analyses. The number and size distribution of released particles depend on many factors, such as mechanical methods used to generate particles, mechanical force speed, number of cycles, applied load, abrasive material, and polymer class and properties. Except for CNTs where bundles of MWCNTs have been observed on released particles for one epoxy system [21], most studies report [28, 29] that nanofillers are still embedded in the released particles. More research is needed to carefully characterize and identify the release entities as a function of nanofiller and material properties, particularly for different classes of polymers.

Because of the concern of release of metal oxide nanoparticles from flooring coatings and interior paints that may potentially have a long-term harmful effects to the occupants, Consumer Product Safety Commission (CPSC) has worked with National Institute of Standards and Technology (NIST) to investigate the potential release by abrasion of nanoparticles from coatings for wood floors and interior paints used in kitchen and bathrooms. Abrasion, as described in a number of ASTM standards for testing the abrasion resistance of coatings and pants, was used to simulate mechanical actions such as walking with shoes, movements of furniture, scratching, and mopping. These mechanical actions have the potential to expose nanoparticles on the floor and painted surfaces as well as release these nanoparticles into the air. Using a variety of analytical instruments and a commercial abrader, the first year of research under this project 1) developed protocols for abrasion of coated and painted samples to generate nanoparticles from floor coatings and interior paints, 2) developed a quick microscopic/image analysis method to quantify the number and size distribution of particles remained on the sample

surface after abrasion, 3) showed that nanoparticle clusters were detectable/visible on the surfaces or embedded in the polymer matrix generated by abrasion through scanning/transmission electron microscopic (SEM/TEM) study [30], and 4) developed a chamber design to quantify the release of airborne nanoparticles from these same abrasion processes [31]. This report describes the second year of research under this project, which has investigated the development of methods and protocols for abrasion of flooring coatings and interior paints in liquid and to measure and identify the particles remained on the surface and in liquid. The year 2 research also investigated the fabrication of a chamber and methods to quantify the number and size of nanoparticles aerosolized in the air by abrasion. The results of the airborne nanoparticle research are described in a separate report [31].

2. Experimental Procedures for Abrasion of Nano-filled Flooring Coatings and Interior Paint in Air and Water*

2.1. Materials and Specimen Preparation

2.1.1. Nano-Filled Flooring Coating and Interior Paint

A commercial water-based polyurethane (PU) coating and a commercial water-based latex interior paint containing an unspecified type and amount of nanoparticles were chosen for this study. Information about these two polymeric materials containing nanoparticles was provided to NIST from a nanoparticle manufacturer, who supplies a majority of nanoparticles to the coatings and paints in the commercial market today. The PU was a typical clear polymer coating used for hardwood flooring, while the paint was a typical interior wall paint for kitchen and bathrooms. Both coatings and paints were purchased at local home improvement stores. There are no inorganic compounds indicated in the material safety data sheet (MSDS) for the PU coating issued by manufacturer. However, according to the nanoparticle manufacturer provider, this PU coating contained small amounts of alumina (Al_2O_3) nanoparticles. The interior paint

* **Disclaimer:** *Certain commercial product or equipment is described in this report in order to specify adequately the experimental procedure. In no case does such identification imply recommendation or endorsement by the National Institute of Standards and Technology, nor does it imply that it is necessarily the best available for the purpose.*

contained the following inorganic compounds: titanium oxide, TiO_2, (10 to 30) % in pigmentary (200 nm to 400 nm) and nanoparticle size, (10 to 30) %; aluminum hydroxide, (1 to 5) %; amorphous silica, (1 to 5) %; nephelene syenite,[†] (1 to 5) %; and a proprietary material, (1 to 5) % (all percentages are by mass), based on the manufacturer data sheet. The sizes of the inorganic materials and chemical compositions of other additives in this interior paint are unknown. Hereafter, the flooring coating and interior paint containing nanoparticles are designated as nanocoating (NC) and nanopaint (NP), respectively.

2.1.2. Wood Substrate

The wood substrates, which were used for both NC and NP, were commercial hardwood plywood panels consisting of a poplar core and red oak veneer faces. It should be mentioned that drywall is commonly used as a substrate for interior paint, as prepared and described in the Year 1 final report. However, because one main objective of this year's work involves abrasion in liquid, the presence of friable, powdery inorganic material of the drywalls would likely confound identification of the particles collected in liquid and those on the abraded specimen surfaces. To avoid these problems, the same wood material was used for both NC and NP. Each wood panel of a dimension of 17.8 cm x 35.5 cm x 5.35 mm (7 inch x 14 inch x 1/5 inch) was cut into three 9.6 cm diameter circular disks that were still attached to the panels, as shown in Figure 1a. This diameter of wood discs is needed to fit in the commercial accessory used for abrading coated specimens in liquid. The center of each disc was drilled to provide a hole having a diameter of 6.25 mm, which was slightly larger than the diameter of the specimen support of the liquid abrasion accessory.

2.1.3. Preparation of Flooring and Painted Specimens for Abrasion

After separating from the wood panel by a cutter, the discs were then inserted in a three circular perforation Teflon mold, as displayed in Figure 1b. The diameter of the perforation was slightly larger than that of the disc so that the latter can just fit in the perforation. The depth of the perforation was about 5.35 mm, which was approximately equal to the thickness of the wood panel. Care was taken so that the surface of the wood discs was at approximately the same level

[†] *Nephelene syenite contains 55 % SiO_2, 22 % Al_2O_3, and 0.6 % TiO_2.*

with that of the Teflon mold. In this way, the thickness of the coating or paint films on the wood substrate was approximately the same for all specimens. Three holes were drilled on the bottom of each mold's perforation to facilitate the dislodging of the coated discs after applying the coating or paint. Flooring coating and interior paint were applied on the wood discs in the Teflon mold using the drawdown technique, as illustrated in Figure 1c. For this process, a volume of viscous liquid coating or paint was spread on one end of the substrate (wood discs in the Teflon mold in this case), and the liquid was drawn down slowly and steadily using a drawdown applicator. This common technique provides a uniform film thickness of polymeric materials on a substrate. After the first coating, each disc was removed from the Teflon mold and dried for 8 h at ambient conditions of 24 $^{\circ}$C and $\approx$ 50 % relative humidity. The coated and painted discs were then inserted back to the mold, and another layer of coating or paint was applied to provide a second layer of floor coating or interior paint. A two-layer coating or paint was used in this study because the wood substrate absorbed a substantial amount of water-based coating and latex interior paint. If one-layer specimens were used, only a very thin layer of coating or paint would be left on the wood surfaces, making the abrasion process more difficult.

The coated and painted wood discs were then cured for two weeks at ambient conditions, as recommended by the manufacturers. The dry film thicknesses of NC and NP were (256 ± 16) µm and (270 ± 28) µm, respectively as measured by a caliper. The coating or paint material in the middle holes of the coated discs was removed by a drill before use. In addition to coated and painted specimens on wood substrate for abrasion studies, free standing films having a thickness of approximately 200 µm were also prepared for evaluating a variety of properties of the coatings and paints. For free standing films, only one coat was applied on a Mylar sheet and cured for two weeks. The free films were easily removed from the Mylar sheets for study

a

b

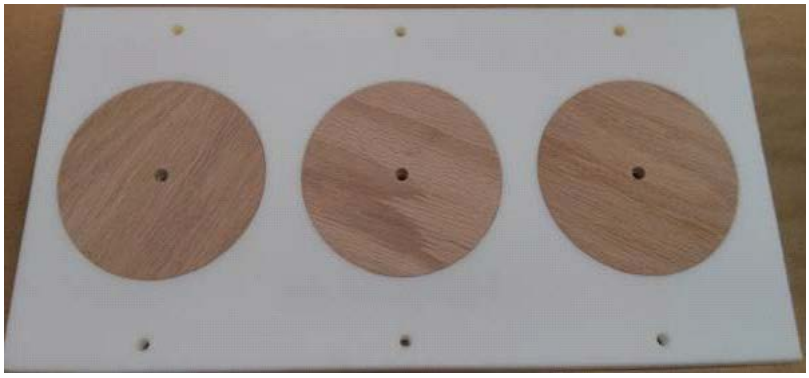

c

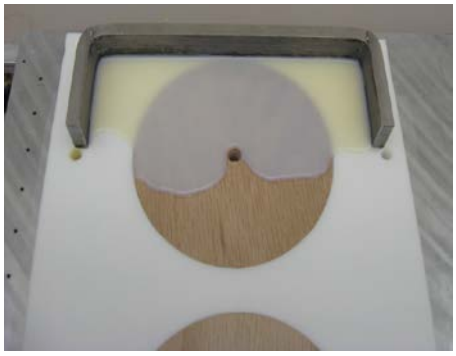

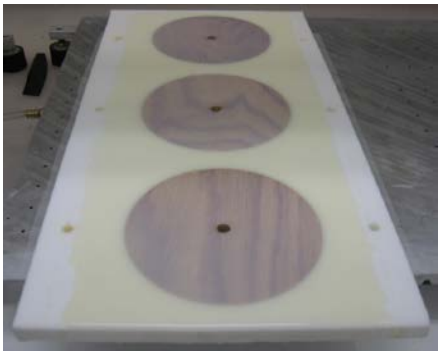

Figure 1. a) Three 9.6 cm diameter discs having a 6.25 mm hole in the center milled from a wood panel, b) 9.6 cm diameter discs inserted in a three circular opening Teflon mold, and c) liquid coating or paint applied to the wood discs using a draw-down approach to generate coated or painted wood disc specimens.

2.2.Instrumentation and Parameters for Abrasion in Water

This study consisted abrasion both in air and in water. The abrasion used the same dual specimen table Taber rotary abraser (Model 5155, Taber, North Tonawanda, NY) (Figure 6 in the first year report) that can abrade two specimens simultaneously, as described previously [30]. This abraser is widely used to evaluate the abrasion and wear resistance of coatings and paints and is specified in several international standards, including ASTM D 4060-95:2007 and ISO 5470-1999. Further, this type of instrument has been used by researchers to study nanoparticle release from polymer nanocomposites due to mechanical forces. The force exerted by the Taber test simulates mechanical forces applied to organic coatings and paints from activities, such as walking, chair movement, polishing actions, and rubbing.

The procedures for abrading specimens in the air were described in the first year report. For the liquid mediated abrasion experiments, distilled water without detergents is served as liquid media. Additional steps for abrading coated and painted specimens in water are illustrated in Figure 2. All abrasions were conducted at a speed of 6.28 rad/s (60 rpm) and 1000 g loading for different numbers of cycles. These abrading parameters were selected as the best practice to generate more particles at the low speed (6.28 rad/s) and high load (1000 g) and detailed results described in previous report [30] and later section. The abrasion operation was performed in a 1.52 m x 0.74 m (60 inch x 29 inch) XPert® Nano Enclosure (LABCONCO, model 3887561) described in the Year 1 report [30].

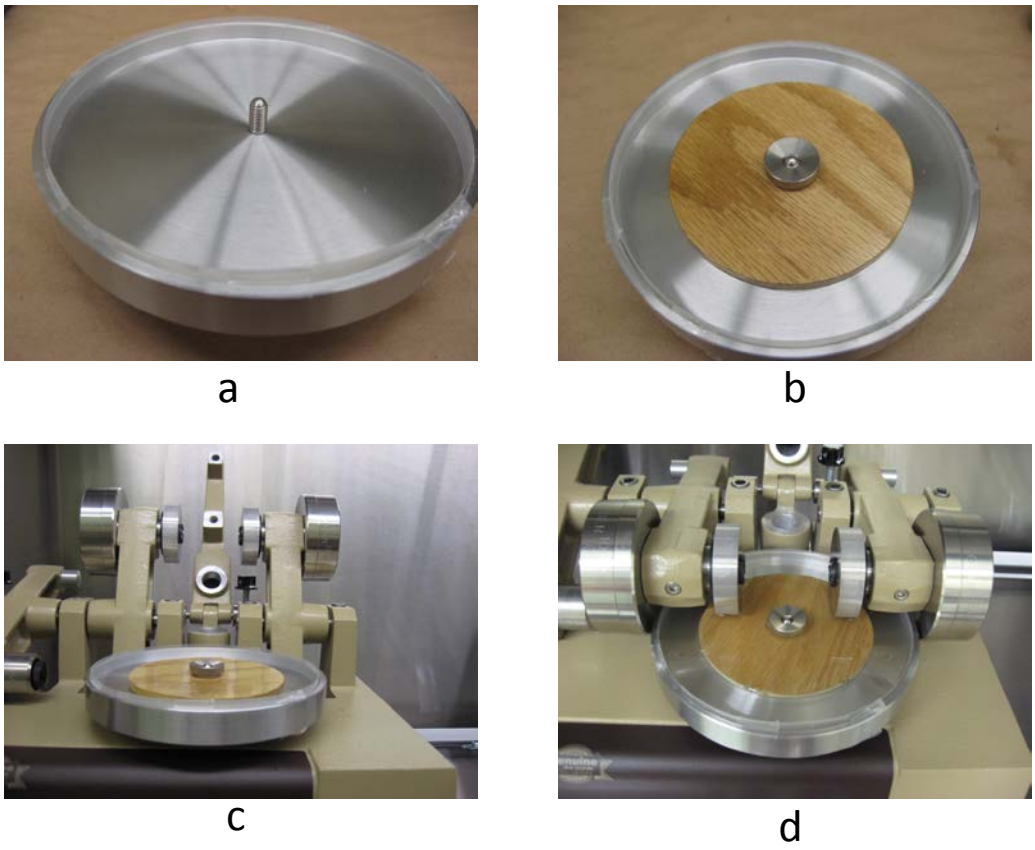

Figure 2. Abrasion in water; a) accessory for abrasion in water, b) a coated wood specimen in the accessory, c) a specimen on the accessory mounted on the rotary Taber abraser, and d) same as c but with addition of distilled water.

In the Year 1 research [30], the commercial wheels were found not to be suitable for studying nanoparticle release because the wheels released particles during abrasion, which interfered with the particles released by the NC or NP samples. One goal of the Year 2 study was to develop an abrasion wheel(s) that is suitable for studying particle released during abrasion of NC and NP in air and in water. The five wheels investigated include:

- CS10: Commercial Taber abrading wheels (mild-medium abrading action); soft and smooth. No mechanical profiling data was measured because it was too soft.
- MW1: A corroded stainless steel wheel (410 SS, which is easy to machine) - 0.0015" (38.1 μm) deep cross patch (MW stands for Metallic Wheel).
- MW2: A non-corroded stainless steel wheel (316 SS, which will not corrode) – 0.00075" (19 μm) deep cross patch.

- MW3: Obtained by polishing MW2 wheel using sand paper.
- MW4: MW3 wheel sandblasted with free silica coal slag blasting abrasives.

Pictures of four of the five wheels are shown in Figure 3 (a picture of the MW3 wheel was not taken before it was sand blasted to make the MW4 wheel). All wheels have the same width and same diameter (10 mm). Here the CS-10 wheel is a commercial wheel, while the other four stainless steel wheels that have specific surface roughness and patterns were fabricated at NIST. The surface pattern of MW1 and MW2 wheels is similar but with different surface roughness. Likewise, the surface pattern of MW4 and the commercial CS-10 is similar. Stainless steel was used because regular steel, although harder, was found to corrode during and after abrasion in water. Surface profiles and roughness values of these wheels are presented in Figure 4. The ranking of surface roughness of the five wheels is as follows: MW1 > MW2 > MW4 > CS10 > MW3. After abrasion, these wheels form a circular band on the coated or painted specimen having a 12.5 mm width and a surface area of approximately 30 cm^2. All results on the number and size distribution of release particles deposited on the coated and painted surfaces were based on measurements in this circular abraded band, because the number of particles outside the abraded band is much smaller (almost zero) compared to those found in the abraded band area, as seen in the first year study [30].

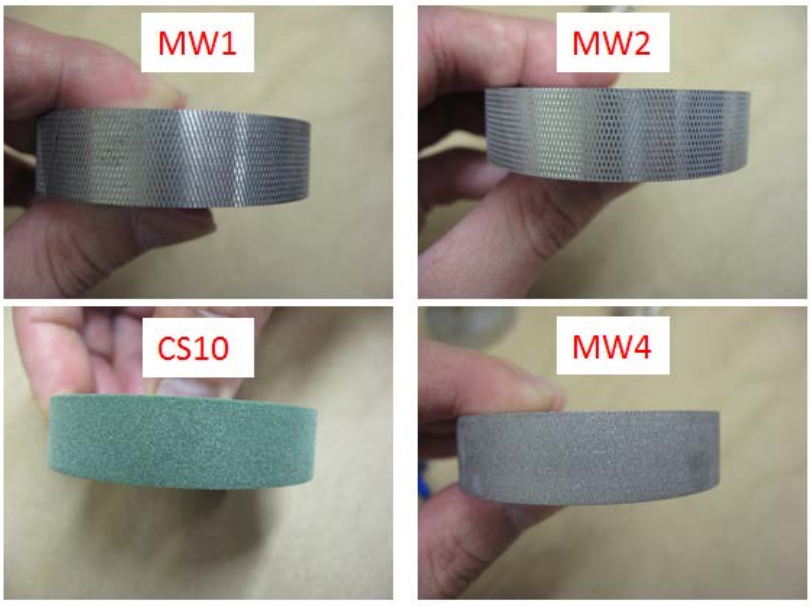

Figure 3. Side view of four of the five wheels used in this study.

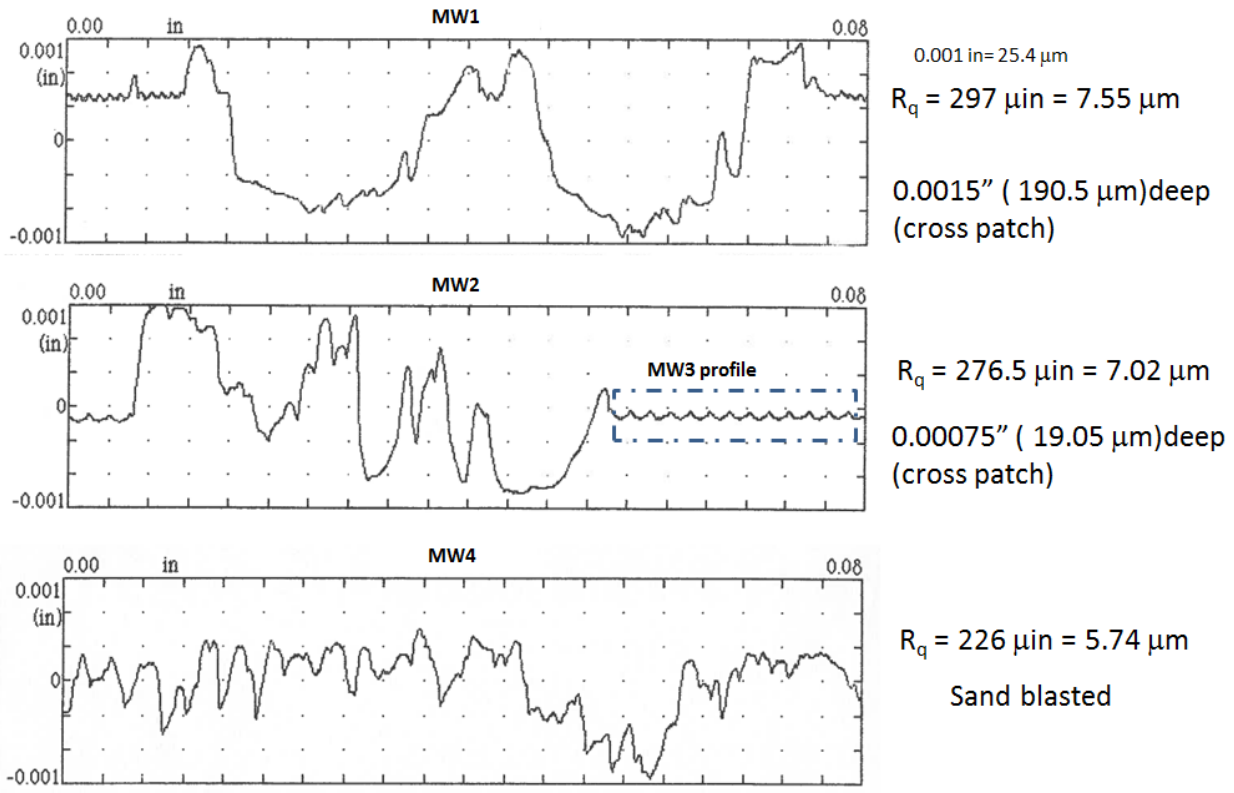

Figure 4. The surface profiles and roughness values of three different metallic wheels: MW1, MW2 (including MW3), and MW4. Here R_q is the RMS (root-mean-square) roughness.

2.3. Characterization of Initial Properties of Flooring Coating and Interior Paint

2.3.1. Surface Morphology

Surface morphology of the nano-filled flooring coating and nano-filled interior paint before abrasion was characterized by laser scanning confocal microscopy (LSCM) and atomic force microscopy (AFM). In addition to measurement of surface morphology of specimens before abrasion, LSCM was the main technique used for quantifying the number and size distributions of particles accumulated on the specimen surface following abrasion in both air and in water. Main features of this technique are given here, with more details on optical microscopy given in the Year 1 report. The laser wavelength chosen in the present work was 543 nm. Multi-scale microstructure measurements of the coatings were carried out using a 150x magnification scale (56.1 µm x 56.1 µm) to a 5x magnification scale (1.7 mm x 1.7 mm). The root mean square (RMS) [32] surface roughness, R_q, was calculated to quantify the morphology changes in surface

and subsurface of coatings before and after abrasion. R_q values presented here are the averaged RMS surface roughness values obtained at 8 measurements (8 measurements from 4 duplicates) from each scanned area of 56.1 μm × 56.1 μm at 150x magnification and 169.4 μm × 169.4 μm at 50x magnification.

LSCM is a fast microscopic technique suitable for imaging particles and their clusters on a specimen surface. When combined with imaging analysis, LSCM can provide quantitative information on the number and distributions of particles having sizes ranging from 80 nm to 10 μm. The freeware *ImageJ* [33] was used with LSCM imaging to obtain data on size distribution of release particles and their agglomerates on the specimen surface. The experimental results provided in the Year 1 report indicated that this microscopic technique is valuable for quantifying the number and size distributions of released particles that are still attached to the specimen surface after abrasion [30]. This method can be used as a screening test for detecting nanoparticle clusters on the abraded surface prior to labor intensive high resolution SEM/TEM microscopic measurements.

LSCM images presented in this report are two dimensional (2D) projections in the X-Y plane, obtained using a regular lens (50x/0.5 or 150x/0.95) method. A typical 2D LSCM image (512 pixel x 512 pixel) was formed by summing the stack of images over the z direction of the film. Pixel intensity represents the total amount of back-scattered light. The bright spots may represent particles with high refractive index on or near the surface while grey regions are associated with the polymeric matrix. Eight micrographs were obtained for each sample (32 micrographs for four duplicates, 8 measurements were selected for total particle counts and surface roughness analyses), with representative images included here. To eliminate the strong reflection from the polymer-air surface, an oil lens (100x/1.3) with a magnification of 100x and a numerical aperture of 1.30 was used to image the particle dispersion inside the coatings. A three dimensional (3D) rendering image, 2D projection images in X-Y plane and X-Z are also presented to illustrate the particle distribution inside the films.

Atomic force microscopy (AFM) is a powerful technique for studying nanoscale features and structures of material surfaces. This instrument can help to identify individual nanoparticles on a specimen surface before and after abrasion. AFM measurements were carried out at ambient conditions (24 ^{o}C, 50 % relative humidity) using a Dimension 3100 system (Veeco Metrology) and silicon probes (TESP 70, Veeco Metrology). Both topographic (height) and phase images

were obtained simultaneously using a resonance frequency of approximately 300 kHz for the probe oscillation and a free-oscillation amplitude of (62 ± 2) nm.

2.3.2. Mechanical Properties and Glass Transition Temperature

Elastic modulus (E) of the flooring coating and interior paint before and after saturation with water were measured using an Instron testing machine at a rate of 10 mm/min until break. For this measurement, Dumbbell (dog bone) - shaped specimens were cut from freestanding films, according to ASTM standard D 638. The thickness of each specimen (used for calculating the modulus) was measured at four different locations. In addition to films cured at room temperature, moduli of films post cured at 120 $^{\circ}$C and those immersed in water were also obtained. These experiments were carried out to determine the effects of post curing and water on the modulus. Reported modulus values are the average of four specimens. Glass transition temperatures (T_g) (transition temperature from glassy state to rubbery state) of these two materials before abrasion were obtained using a dynamic mechanical analyzer (DMTA) (RSA III TA instruments). Measurements were performed from -100 $^{\circ}$C to 150 $^{\circ}$C using a temperature ramp of 3 $^{\circ}$C/min, with a frequency of 1.0 Hz and a strain of 0.5 %. T_g was determined from the maximum of the tan δ peak, and was the average of four measurements (4 duplicates).

2.3.3. Uptake of Water During Immersion and at Different Relative Humidities

To measure water uptake during immersion, specimens having a dimension of 25 mm x 25 mm were cut from free standing films of floor coatings and paints. After weighing to obtain the initial mass, the specimens were immersed in distilled water in separate containers. They were removed from the containers every 2 h except during the night time, blotted (to remove excess water), and reweighed. Water uptake is expressed as, $100x((M_t - M_o)/M_o)$, where M_t is mass of the specimen after immersion in water at time t and M_o is mass of the specimen before immersion to water. The results were averaged for four specimens. For water uptake as a function of relative humidity (RH) (i.e., sorption isotherm), specimens of nanocoating and nanopaint having a mass of approximately (8 to 9) mg, were measured isothermally at 25 $^{\circ}$C using a Hiden IGASorp Moisture Sorption Analyser. The results were the average of three measurements (3 duplicates).

2.3.4. Inorganic Content in Nanocoatings and Nanopaints

Amounts of inorganic material in Nanocoatings (NC) and Nanopaints (NP) were measured using a thermogravimetry analyzer (TGA) (TA instrument). The analysis was carried out in air at a heating rate of 10 $^{\circ}$C/min and a sample size of approximately 7 mg. The results were the average of five measurements (5 duplicates).

2.4. Characterization of Abrasion-induced Surface Release Particles, Abraded Surfaces, and Water Suspended Release Particles

Three kinds of particles are generated during the abrasion of coated and painted samples in air and in water. One type is particles released to the air, hereafter referred to as abrasion-induced airborne release particles or *airborne release particles*. The second type is particles accumulated on the specimen surface following the abrasion in air or water, hereafter referred to as abrasion-induced surface release particles or *surface release particles*. And the third type is release particles suspended in water, hereafter referred to as *water suspended release particles*. The measurement of abrasion-induced airborne release particles was investigated and reported separately in Persily et al. [31]. The characterization of surface release particles, abraded surfaces, water suspended release particles, mass loss and mass of particles suspended in water is reported here. These particles were characterized by LSCM, SEM, inductively-coupled plasma mass spectrometry (ICP), and gravimetric techniques.

Information about the LSCM instrument and procedure for quantifying number and size distributions of release particles on abraded surfaces is provided in the previous section and the first year report. The scanning electron microscopy was performed using a Focused Ion Beam Scanning Electron Microscope (FIB SEM) FEI Helios NanoLab 650. Energy dispersive X-ray spectroscopy (EDXS) was performed using an Oxford Instruments X-Max 80 mm^2 SDD-EDXS Detector. Additional SEM imaging and EDXS for a broader image area was performed using JEOL JSM- 7600F SEM in the Engineering Laboratory. In addition, chemical information of surface release particles and TGA residues was studied by EDXS in the SEM measurements. Particles generated from flooring coating and interior paint generated with the metallic wheel(MW2) were characterized.

The chemical composition and concentration of water suspended release particles after abrasion were analyzed by ICP-optical emission spectroscopy (ICP-OES). The measurement was

performed using the SemiQuant mode of Agilent model 7500cs. The SemiQuant mode is capable of quantifying individual elements. The instrument was calibrated using a solution containing 20 μg kg^{-1} of each of 31 elements prepared by diluting ICP–MS Calibration Standard (Cat# ICP–MSCS) from High Purity Standards with 1.5 % HNO_3. NIST SRM 1643e Trace Elements in Water was used for quality assurance. For this measurement, 50 ml of water containing suspended particles generated from a particular set of abrasion parameters were placed in a polyethylene bottle. Each liquid sample contained a certain amount of precipitates at the bottom of the bottle. Because large particles (> 80 μm) cannot pass through the capillary of the sample introduction device, each sample was decanted to remove the precipitate. If free nanoparticles are present in the solution, they were expected to remain in the supernatant due to Brownian motion. The steps for preparing samples for ICP-OES measurements are described below:

1. Sonicated the samples in the sonicator bath for ≈ 12 min
2. Decanted samples into parts A & B, schematically shown on the left, about 5 h after sonication.
3. ICP-OES measurements were carried out for both part A & part B.

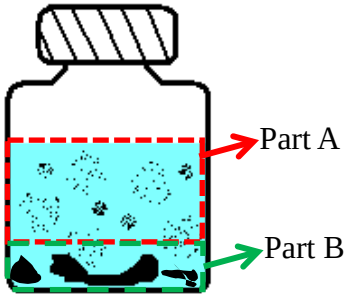

The mass of the decanted solutions (upper portion) usually ranged between 50 g and 60 g. After separation, concentrated HCl was added to both the upper and lower portions (0.6 ml and 1.5 ml, respectively), and these solutions were partially evaporated using a hotplate. The acid was added to aid in dissolution of the nanoparticles and extraction from the polymer. The final solutions contained 3 % to 6 % HCl and were analyzed using ICP-OES. The analytes (Al, Si and Ti) were quantified using the method of standard additions.

In addition to flooring coating and interior paint samples abraded at different cycles, a number of controlled samples were also measured by ICP-MS to ascertain that the elements obtained are those from the nanocoating (NC) and nanopaint (NP) samples. These "*controlled*" samples were:

A. Distilled water alone
B. Water + liquid abrasion accessory (water, but no sample, placed in the accessory for 5 min, which is the time required to complete 160 cycles)

C. Water + wood + accessory (water placed in the accessory containing the wood disc for 5 min)
D. Water + nanocoated wood + accessory (water placed in the accessory containing the nanocoated wood disc for 5 min)
E. Water + wheel (water having wheel immersed for 5 min)
F. Water + nanopainted wood + accessory (water placed in the accessory containing the nanopainted wood disc for 5 min)

The mass of release particles suspended in water was measured as described below. Before abrasion, the mass of each specimen was measured using an analytical balance having a mass resolution of 10^{-5} g. After completing the abrasion over a predetermined number of cycles, the entire water volume (90 ml) with suspended release particles in the water abrasion accessory was transferred to a pre-weighed beaker by the use of a pipette. Another 30 ml of water was then added to the just emptied accessory (to further remove particles attached to the accessory's wall). After transferring the 30 ml additional water to the beaker already containing water suspended particles, the beaker was placed in a 70 $^{\circ}$C oven. After all water was evaporated, the mass of the beaker containing dried release particles was measured, and the mass of the particles suspended in water was then obtained. The results were the average of three measurements (3 duplicates).

The mass loss of each specimen after abrasion in air was obtained by simply weighing the specimens before and after abrasion, similar to the approach used in industry for studying abrasion and wear resistance of organic coatings and paints. The results were the average of three measurements (3 duplicates).

3. Results and Discussion

3.1. Initial Properties of Nano-filled Flooring Coatings and Interior Paints

3.1.1. Morphology and roughness of flooring coating and interior paint surfaces before abrasion

Surface morphology and roughness of a material play an important role in the abrasion behaviors of polymeric materials [32]. AFM and LSCM images of NP and NC surfaces before

abrasion were characterized and the results are displayed in Figures 5 through 6. Figure 5 shows both topographic and phase AFM images of (a) NC and (b) NP at three different magnifications. The AFM phase imaging is a useful technique for distinguishing domains that have different mechanical and chemical properties, such as inorganic nanoparticles in polymer matrices. The Phase images show the presence of particles on the surface of both the NC and NP samples, with some particles having nanoscale dimensions.

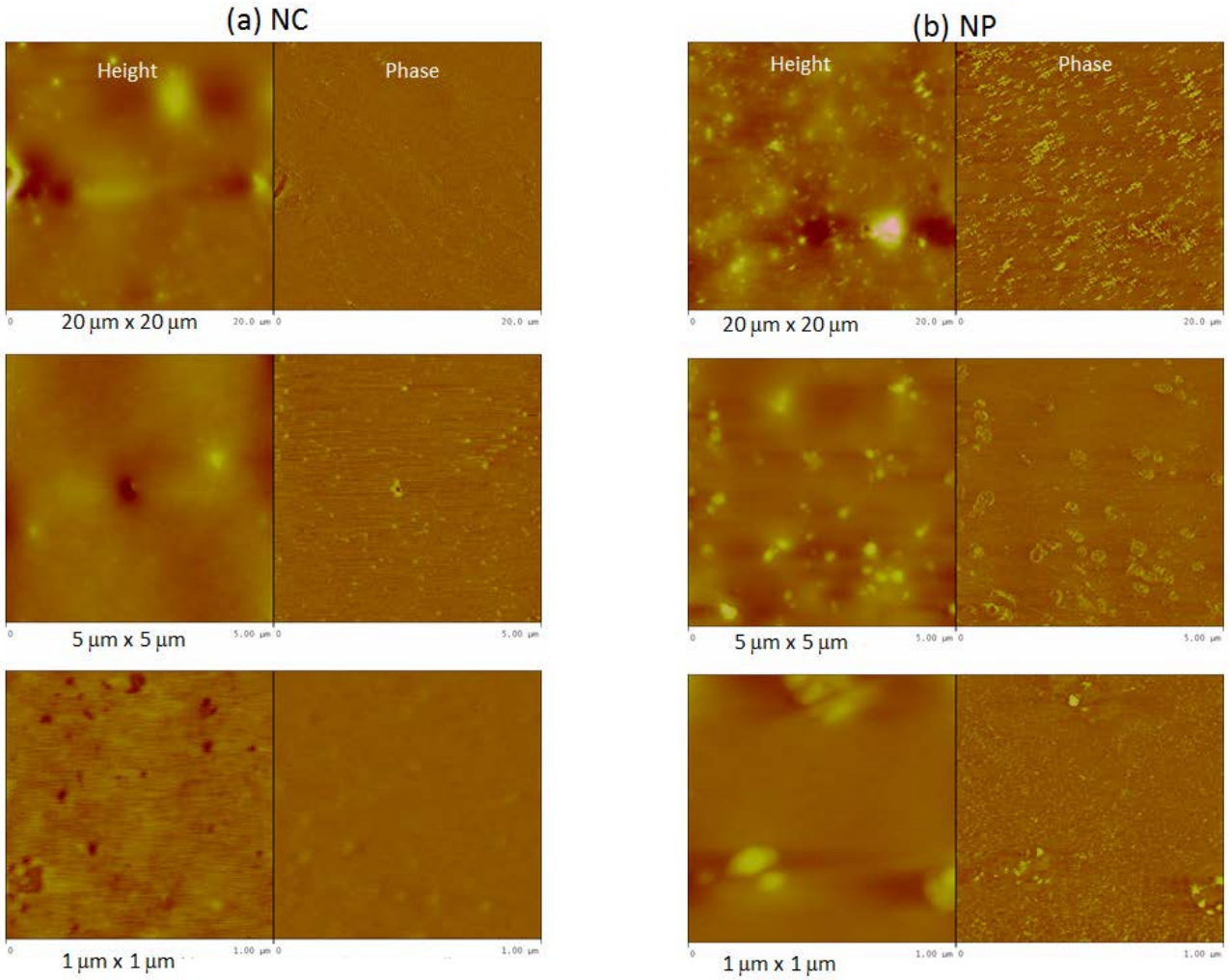

Figure 5. AFM images of (a) NC and (b) NP at three different magnifications, as indicated in the graphs. For each AFM pair, the height image is on the left and phase image is on the right.

Figure 6 displays surface morphology and subsurface features in 3D, X-Y, X-Z 2D LSCM images. LSCM images of NC sample (Figure 6a) show some large particles on its

surface, and many large agglomerates near the surface using the oil lens imaging method. Noticeably, the Z value, the total scanning or laser penetration depth, in the X-Z projections of NC is very different from that of NP sample (Figure 6b): 60 μm vs. 6.8 μm. Generally speaking, a smaller Z value implies the coatings contain uniformly distributed and densely packed particles near the surface layers, which scattered most of the incident laser light near the surface, preventing the laser from penetrating deeper, while a larger Z value indicates the coatings containing fewer, larger particles packed loosely near the surface. The LSCM images indicate that the subsurface morphology/microstructure in NP displays a better dispersion than that of NC. Note that the two materials are very different: the TiO_2 particles in the NP have a higher index of refraction compared to nanoparticles in the NC and the particle concentrations in NP are much higher than NC.

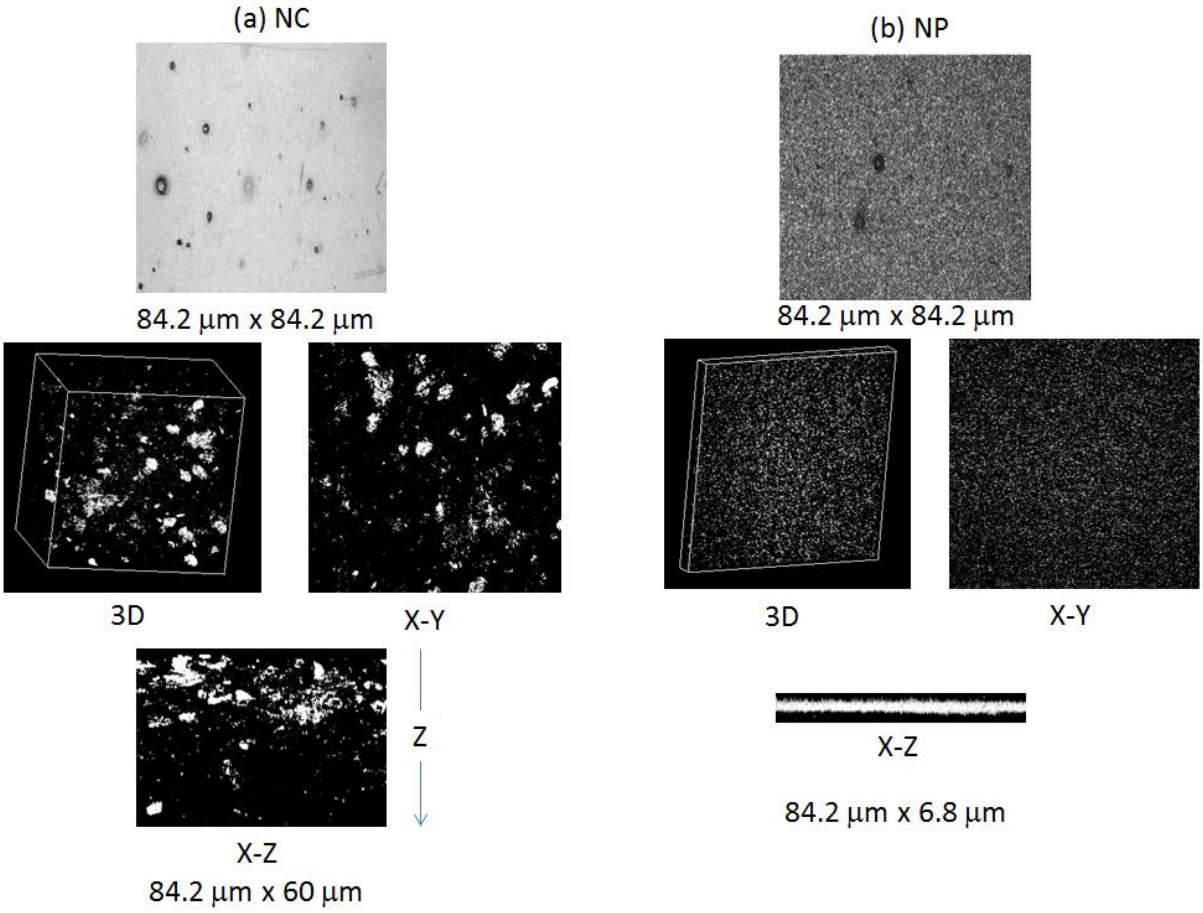

Figure 6. LSCM images of (top graph) 2D (X-Y) and (middle & bottom graphs) 3D, 2D (X-Y, X-Z)– measured by an oil lens imaging method for (a) NC and (b) NP.

3.1.2 Mechanical Properties

Similar to surface morphology, mechanical properties of a polymer, particularly modulus and stress/strain behavior, have a strong influence on its abrasion and wear behaviors [32]. Representative stress-strain curves of NC and NP are presented in Figure 7a. These two materials show typical properties of a plastic material, i.e., they go through a yield region and a long elongation before breaking. Such behavior gives a large area under the curves, indicating a high toughness. The modulus of each material was obtained from the slope of the early portion of their respective curves, as shown on the right of Figure 7b. The modulus and tensile strength values (average of three specimens) of the NC and NP are included in Table 1. The moduli of NC and NP were (325 ± 15) MPa and (9.4 ± 0.69) MPa, respectively and the tensile strength of the NC was three and a half times greater than that of the NP. The modulus of the NP is low, typical for elastomeric and rubber materials. However, its elongation at break was more than five times greater than that of the NC.

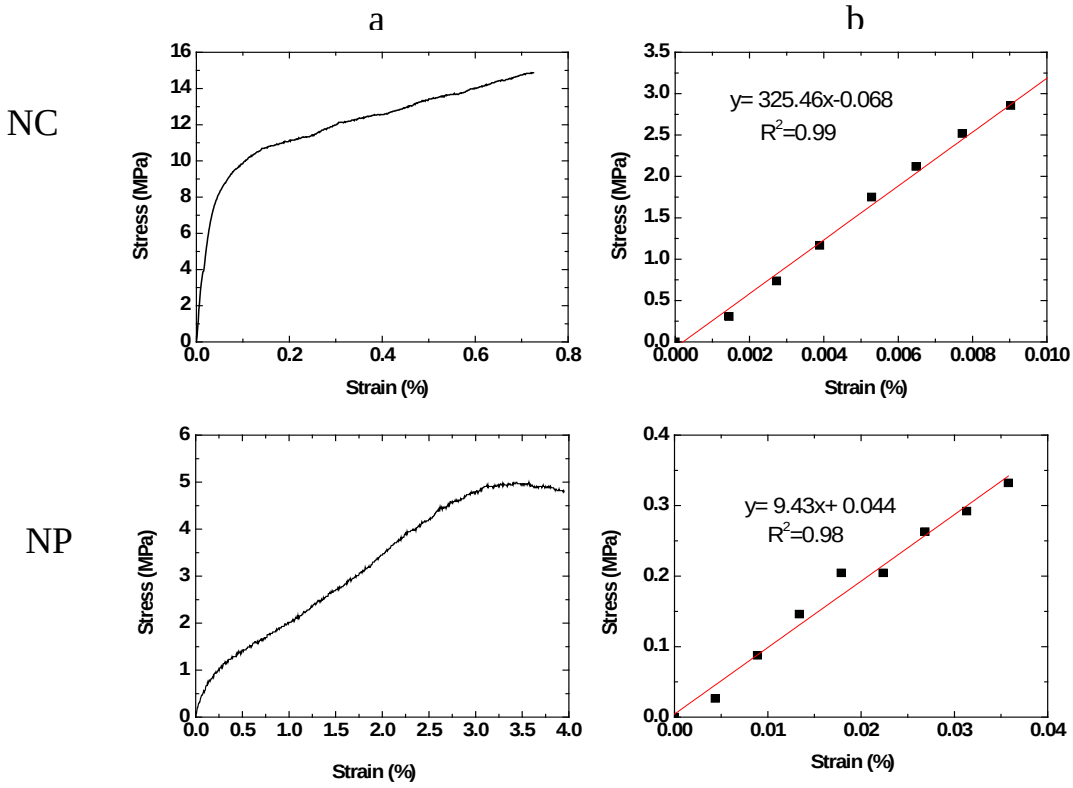

Figure 7. (a) Representative stress-strain curves of NC (top) and NP (bottom), and (b) expanded early portion of their respective stress-strain curves for obtaining modulus of elasticity.

Table 1. Initial properties of NC and NP used in this study. The uncertainties represent one standard deviation from at least 3 duplicated samples.

Property	NC	NP
Specimen thickness, µm	253 ± 16	270 ±18
Density, g/cm^3	1.15	2.33
Young modulus, MPa	325 ± 15	9.4 ± 0.69
Young modulus water saturated, MPa	71.4 ± 4.0	----
Tensile strength, MPa	14.35 ± 0.37	3.78 ± 0.31
Tensile strength water saturated, MPa	5.59 ± 0.43	----
Diffusion coefficient, D, 10^{-13} m^2 t^{-1}	3.6	10
Glass transition temperature, T_g, °C	87.5 ± 1.0	4.9 ± 0.6
Inorganic Solid content (TGA), %	(0.26 ± 0.01)%	(37.75 ± 0.90)%
Water uptake, %	(11.72 ± 0.8)%	(56.67 ± 3.35)%
Surface roughness, µm	2.10 ± 0.02	3.48 ± 0.27

The effect of water on the stress-strain behavior of the NC is shown in Figure 8 (this measurement could not be performed for NP because it was too soft after immersion in water). The lower curve is from NC that was immersed in distilled water for 24 h. This time period was required to saturate the 250 µm thick NC free film (see the water uptake section, 2.3.3). As shown in Figure 8, both the ultimate tensile strength (at break) and the modulus of the NC

decreased substantially after immersion in water. The values of tensile strength and modulus of NC after saturating with water are also included in Table 1. The tensile strength and modulus values after water saturation were less than half and one quarter, respectively, of their initial values. This substantial decrease in mechanical properties will likely have a strong effect on the behavior and the number of release particles during abrasion of NC in water. This information is vital, yet essentially no data about the effects of water in coating or paint films on their abrasion behavior is available. Further studies on the effects of water uptake on the abrasion behavior of NC and on particle release are needed.

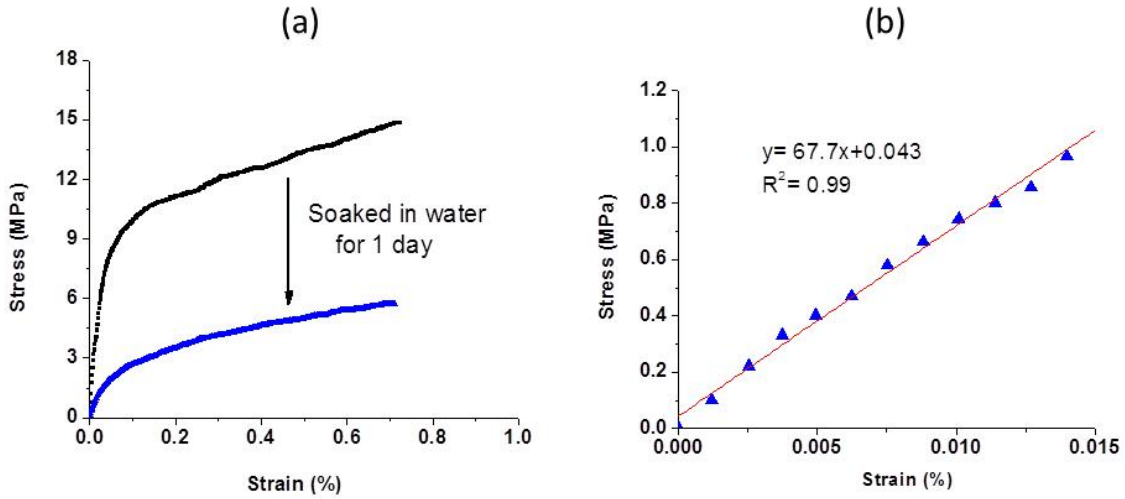

Figure 8. a) Stress-strain curves of NC before (upper) and after immersion in water for one day (lower), and b) expanded early portion of the lower curve.

3.1.3 Water uptake during immersion and as a function of RH

The effects of water on the mechanical strength of the flooring NC are given above. The presence of water in a polymer film on a substrate will also cause swelling, plasticizing, blistering, and debonding (delaminating from the substrate), which will likely affect the abrasion behavior and nanoparticle release from the coated or painted surfaces. Further, for hydrolysis-susceptible polymers such as polyesters, acrylic melamine, polyamides (nylon), and biocompatible polymers, water will cause irreversible degradation of these materials, potentially triggering a release of nanoparticles from the polymer nanoproducts. Such a release of carbon nanotubes by hydrolytic degradation of biocompatible polymers in biological fluids has been observed and is included in a recent review of nanoparticle release [35]. Figure 9a depicts the process and relative quantities of water uptakes in NC and NP. Freestanding films were used for

these measurements. The thickness of the NC film was (253 ± 16) μm and that of the NP was (270 ± 18) μm. The averaged values are from 4 duplicates and the uncertainties (±) represent one standard deviation. Both materials absorbed water readily and quickly. It took approximately 20 h for water to reach the equilibrium (saturated) in the NC, but it required more than 4 times longer to saturate the NP. Further, the maximum water uptake in NP was greater than 55 %, near 5x that of the NC (≈ 11.7 %). This result can be partly explained by the fact that the NP is a latex paint containing nearly 37 % inorganic materials, whereas the NC contains little inorganic materials. In addition to containing sites on the polymer chains and inorganic particles surface for molecular water to adsorb on, the NP also contains large amount of inorganic material and latex particle interspaces would provide voids that will take up liquid water. Thus, in addition to physically adsorbed water molecules, water-saturated NP also contained a substantial amount of liquid water. The values of maximum water uptake for NC and NP are also included in Table 1.

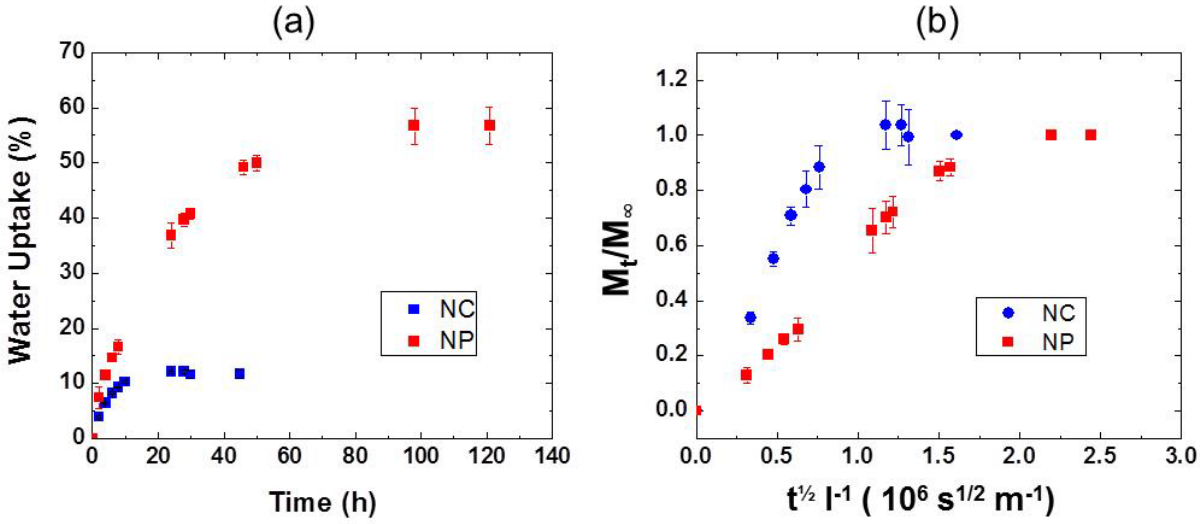

Figure 9. a) Water uptakes in NC and NP, and b) their M_t/M_∞ vs $t^{1/2}\ l^{-1}$ curves. The error bars represent one-standard deviation.

The water uptake (i.e., sorption) data were used to calculate the Fickian diffusion coefficient of water, D, for NC and NP. Diffusion coefficients were determined from the M_t/M_∞ vs. $t^{1/2}\ l^{-1}$ curves shown in Figure 9b, which is the most common method to calculate D from sorption data [36]. M_t and M_∞ are the masses of water uptake at time t and infinity (i.e., at

saturation), respectively, t is the immersion time in water, and l is the film thickness. M_t and M_∞ values for the two materials were taken directly from Figure 9a. D was calculated using $M_t/M_\infty = 0.6$, which is the linear part of the curves in Figure 9b. D values of NC and NP are given in Table 1, which shows that D of the NC is almost three times greater than that of the NC. These D values are useful for estimating how far and how fast water can penetrate into the two materials at a given period of time.

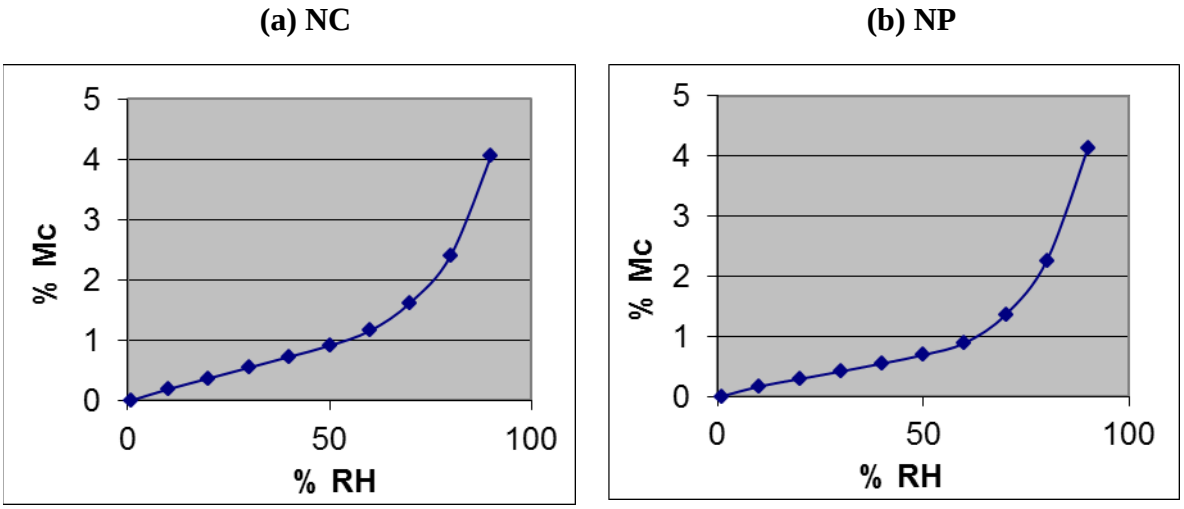

Figure 10. Water sorption isotherms: a) NC, and b) NP.

In addition to water uptake during immersion, the amounts of water adsorbed as a function of relative humidity (RH) (i.e., water sorption isotherm) for NC and NP were also measured, and the results are displayed in Figure 10. The moisture content, Mc, on the vertical axis (Figure 10) has the same definition as that for the water uptake during immersion shown in Figure 9a. It is interesting to observe that despite a marked difference in the amounts of uptake during immersion in liquid water, these two nanoproducts have similar sorption isotherms: water vapor was adsorbed slowly between 0 % and 60 % RH, but rose more rapidly between 70 % and 90 % RH. At 90 % RH, nearly 4 % of water was taken up in both materials. These water sorption isotherms are useful for estimating the amount of water in NC and NP when ambient RH is known. As indicated above, the presence of water, both adsorbed water and liquid (absorbed) water in the film plays an important role in the mechanical, physical and chemical properties of polymeric materials. Adsorbed water causes physical changes such as swelling and plasticizing of the polymer structure, as indicated earlier. On the other hand, although liquid

water does not contribute to the swelling or plasticizing of the polymer films, it causes blistering and debonding and is the main reactant in hydrolytic degradation.

3.1.4. Inorganic Contents and Their Chemical Composition in Nanocoating and Nanopaint

The amounts of inorganic materials, including nanoparticles, in NC and NP were determined by the TGA technique, and representative results are displayed in Table 1. Because the inorganic content in the NC was small, an expanded TGA curve (inset) is included for this material. The mass losses between 100 °C and 300 °C in both NC and NP were due to residual water/solvent and low molecular mass materials, such as plasticizers, surfactants, etc. The high molecular mass polymer chains in both materials started to lose mass (decompose) around 300 °C. The mass loss was rapid between 300 °C and 500 °C for the NC and between 300 °C and 400 °C for NP. Further, the mass loss of the NC did not reach a constant value until around 650 °C while that of the NP reached a plateau 400 °C. A close examination of the TGA curves of the NC (Figure 11a) revealed that this material still retained approximately 7 % residue at 500 °C and that the mass loss rate between 500 °C and 650 °C was slow. Such behavior, particularly the mass loss at relatively high temperature, suggests that the NC is more thermally stable than the NP. Note that NP is a waterborne latex paint, which cures very slowly and thermal properties have constantly changed.

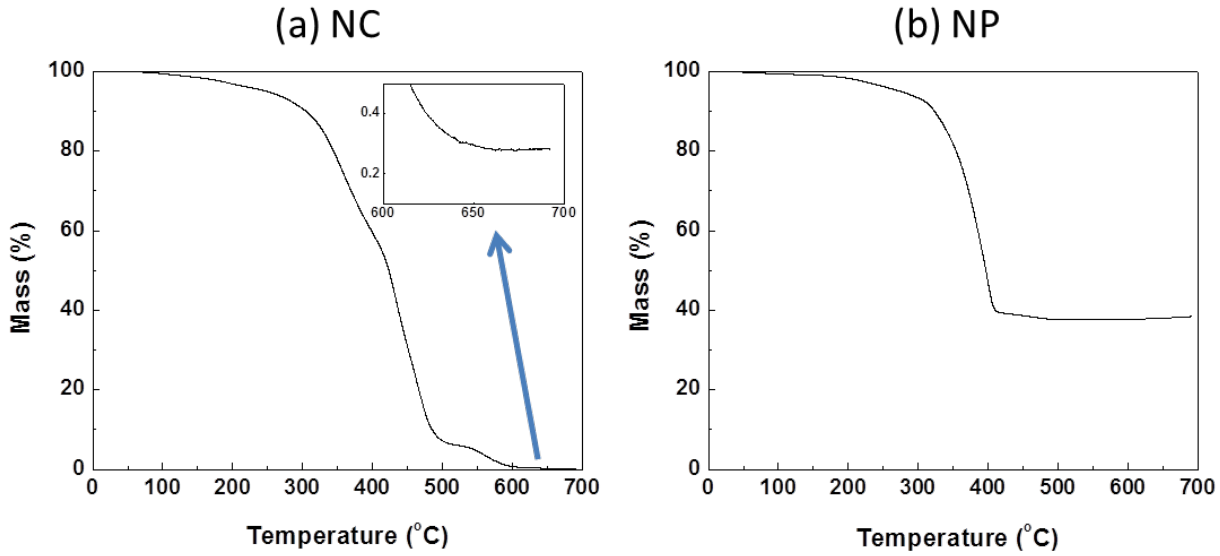

Figure 11. Representative TGA curves of (a) NC and (b) NP.

Because the TGA measurements were conducted in air, all organic material in the sample was assumed to completely decompose by combustion at 700 °C. Note that any residue between the temperatures at which the organic polymer was totally decomposed (around 400 °C to 500 °C, which varies with polymers) and 700 °C was due mainly to the inorganic content. Thus, it is expected that no organic material was left in the TGA residue obtained in this study. However, the highest temperature in TGA measurement was 800 °C, which is not high enough to cause Al in the metal-oxide Al_2O_3 to be vaporized. From the TGA curves such as displayed in Figure 11a and Figure 11b, total inorganic contents in NC and NP were (0.26 ± 0.01) % and (37.75 ± 0.90) %, respectively. These values, which were the average of three specimens, are included in Table 1. Because only nanoparticles were assumed to be present in the NC, the (0.26 ± 0.01) % represents the total amount of nanoparticles in this material. On the other hand, the (37.75 ± 0.90) % in the NP composes of nanoparticles and several other larger particles, such as pigmentary TiO_2 (diameter: 200 nm to 400 nm), amorphous silica, etc., as given in the experimental section.

To identify chemical composition of the inorganic materials in the NC and NP, EDXS with SEM was employed to characterize 1) the TGA residues and 2) film cross sections of the two materials. For EDXS analysis of the TGA residues, a copper sheet was laid on the bottom of the TGA sample pan before loading the sample. After the TGA run, the copper sheet having the residue on it was removed from the sample pan and the residue characterized. The copper sheet placed at the bottom of the sample pan was used because a preliminary study indicated that the residues adhered strongly to the bottom of the TGA platinum sample pan and could not be removed for characterization by EDXS or SEM.

Figures 12 and 13 display SEM images and EDXS spectra of the TGA residues of NC and NP. For the NC, Spectrum 2 (from location #2 in the SEM image, Figure 12) of the TGA residue, which was collected from a location outside of the residue material, exhibits mostly Cu and O from the oxidized copper surface, as expected. On the other hand, Spectra #1 and #3 of the same TGA residue show, in addition to Cu and O, a substantial amount of Si and a minor amount of S and P. These results suggest that the TGA residue of the NC contained mostly silicon-based material. For the NP, all its three EDXS spectra (Figure 14) of the TGA residue exhibit a high concentration of Ti with Al, Si and Cu as the minor components. These results are consistent with the manufacturer data sheet, which contain (10 to 30) % titanium oxide, (1 to

5) % aluminum hydroxide, and (1 to 5) % amorphous silica, as given in the experimental section. Again, the Cu is from the copper sheet.

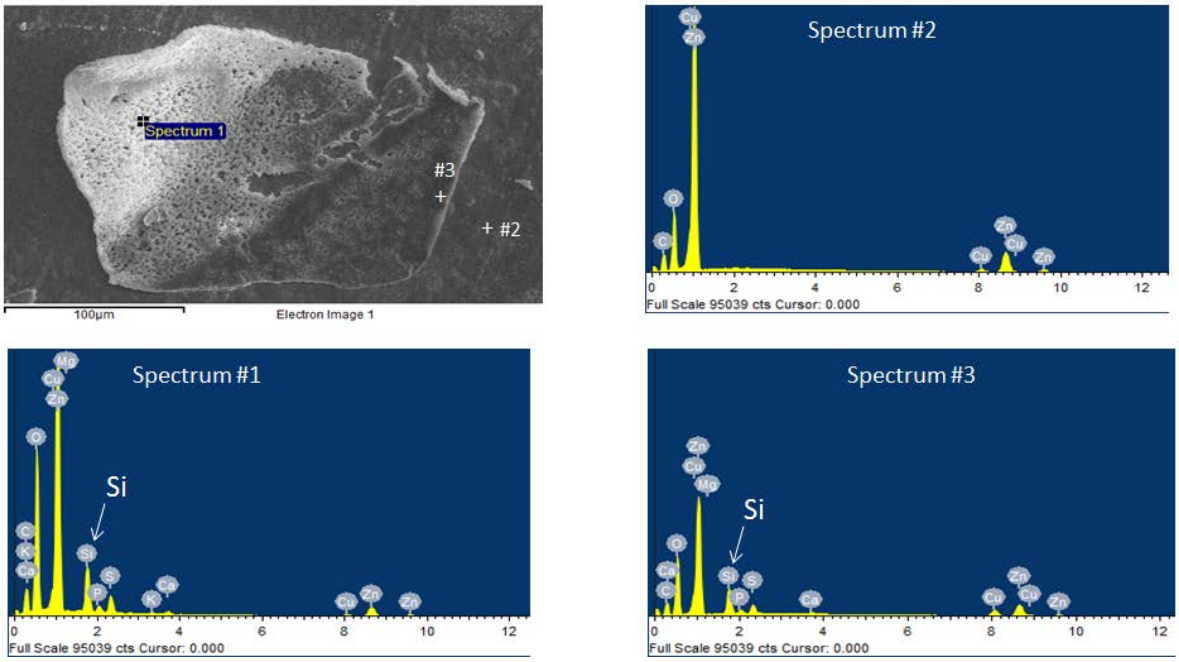

Figure 12. EDXS spectrum on NC residues obtained after TGA measurement.

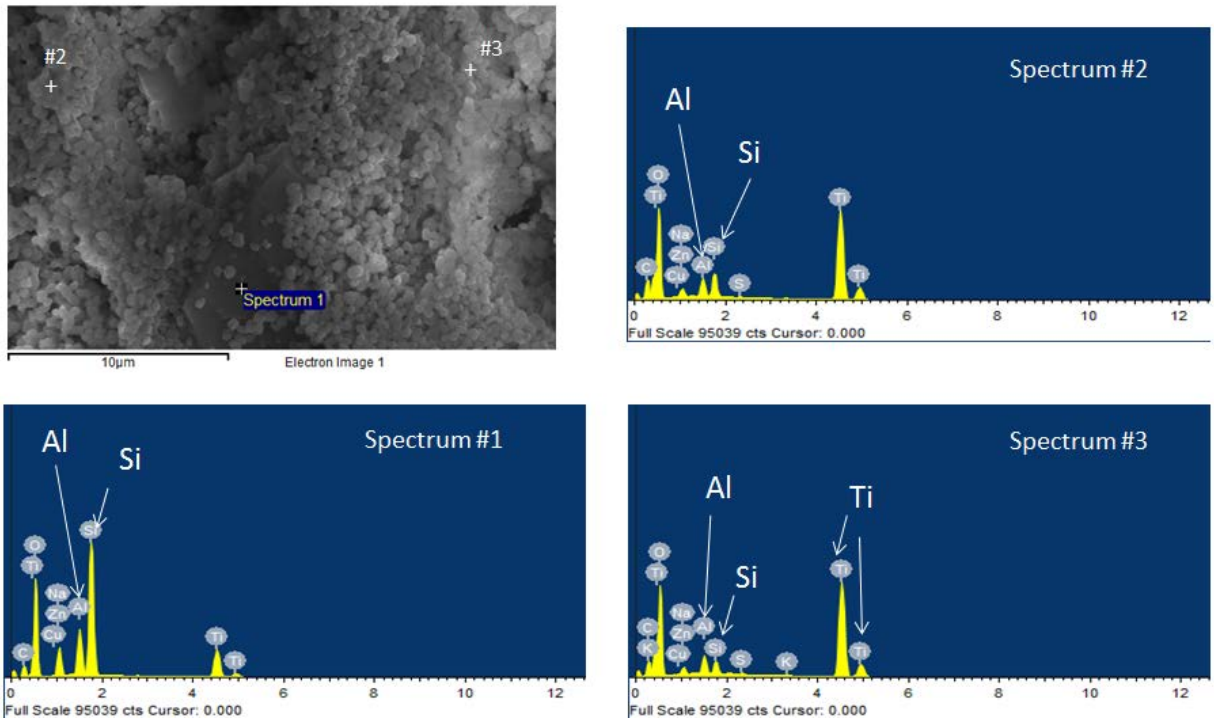

Figure 13. EDXS spectrum on NP residues obtained after TGA measurement.

To determine the presence of nanofillers in the NP, high magnification SEM images of its TGA residue were obtained, and the results are displayed in Figure 14**.** Except for a few particles that have a 130 nm size (Figure 14b), most particles in these images have a dimension typical of pigmentary TiO_2, i.e., in the 200 nm to 300 nm range, with no evidence of TiO_2 nanoparticles, which have a size between 30 nm and 40 nm. One possible explanation is TiO_2 nanoparticles, which are more surface energetic than coated pigmentary TiO_2, agglomerated after the organic polymer was removed by combustion. Further imaging on other NP TGA residues needs to be carried out to confirm this results/hypothesis.

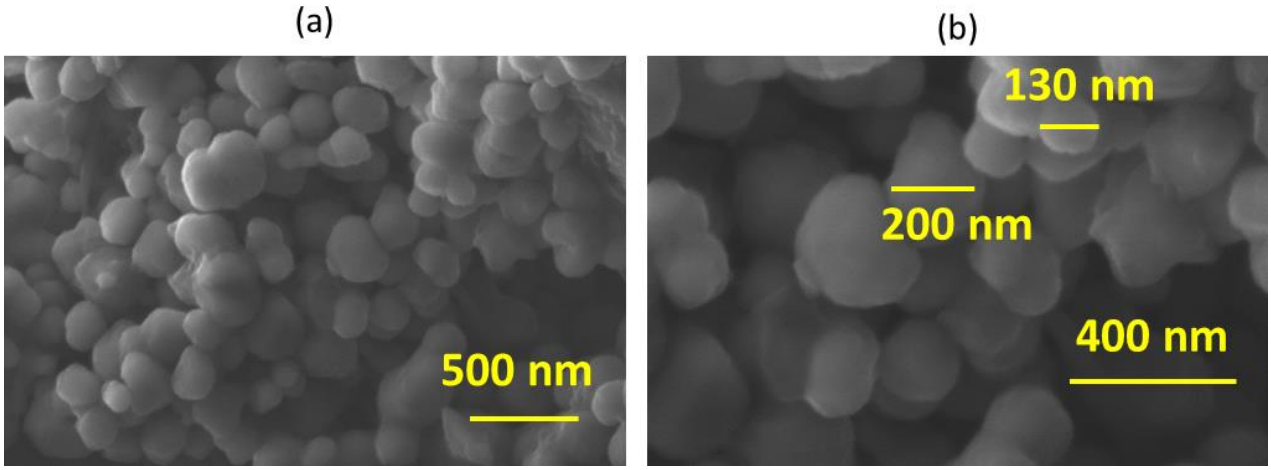

Figure 14. High magnification SEM images of NP TGA residue; a): 50 K, and b) 100 K.

Figures 15 and 16 display SEM images and EDXS spectra obtained from the cross sections of NC samples. EDXS spectra of Figure 15 were collected from four different locations indicated in the SEM image (Figure 15, left), while the EDXS spectrum in Figure 16 (left) was obtained from the entire SEM image shown on the right of Figure 16. Except for Spectrum #1, which shows the presence of Na and Cl probably from contamination, all four EDXS spectra in Figure 15 exhibit C and O as the major components, as expected for the polymeric materials, and Al and Si as the minor components. On the other hand, the EDXS spectrum in Figure 16 displays, in addition to C and O, a high concentration of Al with Si and S as minor components. The presence of Al and O elements is consistent with information from the NC manufacturer that the flooring NC contained alumina nanoparticles (Al_2O_3), but does not agree with the EDXS results of the TGA residue shown in Figure 12, which revealed the presence of Si but little evidence of Al. The reason for this difference is unknown and is being investigated.

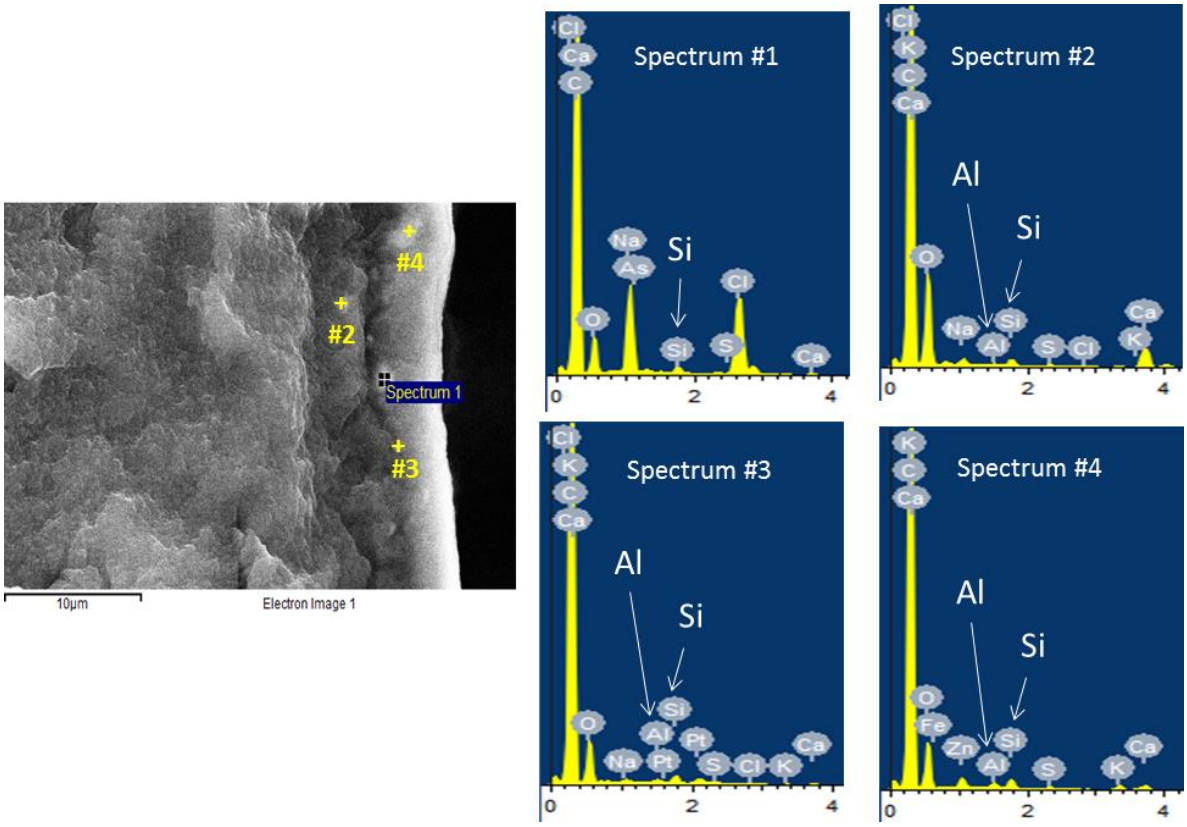

Figure 15. SEM image (left) and four EDXS spectra (right) from a NC sample cross section (the locations where the spectra were collected are indicated in the SEM image).

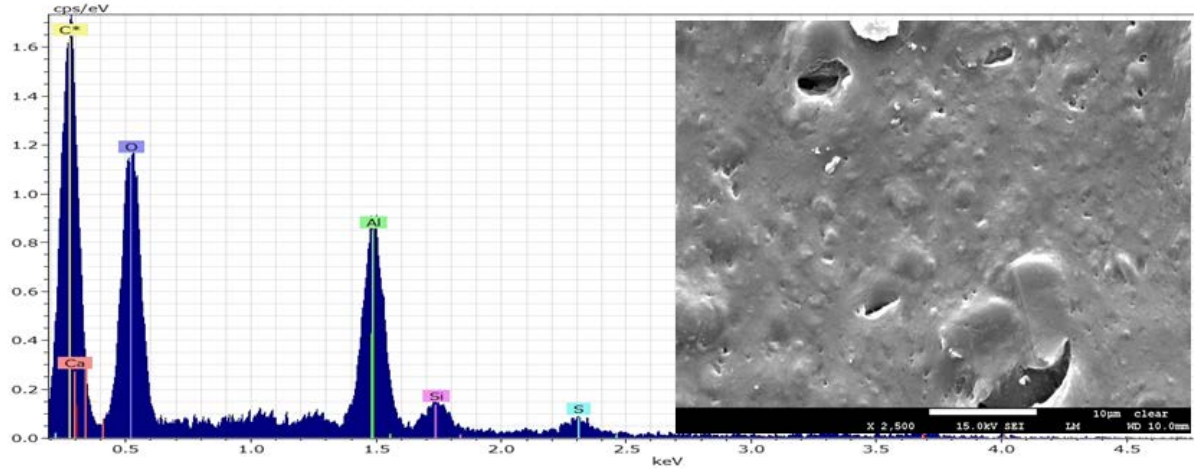

Figure 16. An EDXS spectrum (left) obtained from the entire SEM image (right) of a NC sample cross section.

3.2. Effect of Wheel Type on Surface and Water Suspended Release Particles

3.2.1. Surface Release Particles by Dry Abrasion

As stated in the experimental section, common commercial abrasive wheels, which are composed of alumina or silica particles embedded in a rubber binder, are not suitable for studies of nanoparticle release from NC or NP by mechanical forces. These wheels release their own particles during abrasion which cannot be separated from those released by the tested sample. To avoid this problem, in Year 1, we investigated the use of a commercial tungsten wheel for generating release particles from NC and NP by abrasion. However, due to released particles from the samples becoming embedded in the wheel's deep and large grooves, the commercial tungsten wheel was also found to be unsuitable. Nevertheless, the hard metallic tungsten provided encouraging results in that the wheel itself did not release its own particles. Based on these results, an investigation on the use of metallic wheels having different surface patterns and roughnesses for particle release was included in Year 2 study. The main objective of this study was to find a wheel or wheels that have an appropriate surface profile (surface roughness and pattern) to effectively abrade polymer NC and NP, without generating its own particles during either dry and wet abrasion. Such a wheel(s) could become a "*standard*" or a recommended wheel for studies of nanoparticle release by the mechanical forces applied to nanocoated and nanopainted surfaces, such as walking, wiping, mobbing, polishing, and furniture movements. Pictures of these metallic wheels studied and their composition and surface profiles are given in the experimental section (Figures 3 and 4). In addition to the four metallic wheels (MW1, MW2, MW3, and MW4) that have different surface patterns and roughness values, a commercial wheel widely used for evaluation of coatings, CS10, was also included for comparison.

In Year 1 [30], the effects of abrading parameters, such as abrasion speeds: 7.53 rad/s (72 rpm) vs. 6.28 rad/s (60 rpm), applied loads: 500 g vs. 1000 g, and abrasion cycles: 100, 200, 300, 400, 500, on the number and size distribution of release particles accumulated on the surfaces were also examined. The results indicate that 1) the higher load also appeared to generate more particles than the lower load; 2) the number of cycles had a minimum effect on the surface release particles for all sizes at 7.53 rad/s (72 rpm) speed; however, the number of cycles appears to have a noticeable effect at 6.28 rad/s (60 rpm), with the highest number of

cycles yielding the smallest number of particles, both for the total number and for each size from 0.1 μm to 0.4 μm. This result may be due to the non-uniform particle distribution in the Z-direction and a gradient from the surface. In summary, it was selected as the best practice to generate more particles at the low speed (6.28 rad/s) and high load (1000 g). Per previous study, Year 2 research only focused the effect of abrading cycle on the number or size distribution of release particles accumulated on the abraded surface at a fixed speed and load. The repeated abrasion action on the specimen surface may strongly influence the number or/and distribution of surface release particles.

Figures 17 displays representative LSCM images taken at two different magnifications for NC surfaces abraded using the five wheels. These images were obtained from dry abraded NC specimens at 6.28 rad/s (60 rpm), 1000g load, and 100 cycles. As indicated earlier, the bright regions in a LSCM image are due to the greater reflection from the objects that are above the surface, and the darker regions represent the objects that are below the surface. Thus, the bright particles observed in these images are believed to be loose particles generated by the abrasion, i.e., surface release particles (release particles deposited on abraded surfaces), as defined before. This chacterization was confirmed in the Year 1 study by the use of a pressure sensitive adhesive tape applied on the abraded surfaces followed by LSCM imaging on both the tape and abraded surfaces. In Figures 17 the number beneath each image is the RMS roughness value, in μm, for the entire scan area, and the number that follows the ± sign is one standard deviation. All roughness values were the average of 8 images/measurements from 4 duplicates.

The surface roughness values of NC abraded by the five wheels using the LSCM 169 μm x 169 μm scan size (50x) are presented in Figure 18 (larger scan size generally represents the average surface roughness better than smaller scan size). Despite a marked difference in their surface profiles, the MW1 and MW2 wheels yielded essentially the same abraded surface roughness. The roughness obtained by the MW4 wheel is between those of MW1 or MW2 and CS10. Further, the MW3 wheel produced the smoothest abraded surface, as predicted based on the surface profile shown in Figure 4. Surface roughness of NC abraded by the five wheels has the following decreasing order: MW2 ≈ MW1 > MW4 > CS10 > MW3. This result is consistent with the mechanical profile measurements in section 2.2.

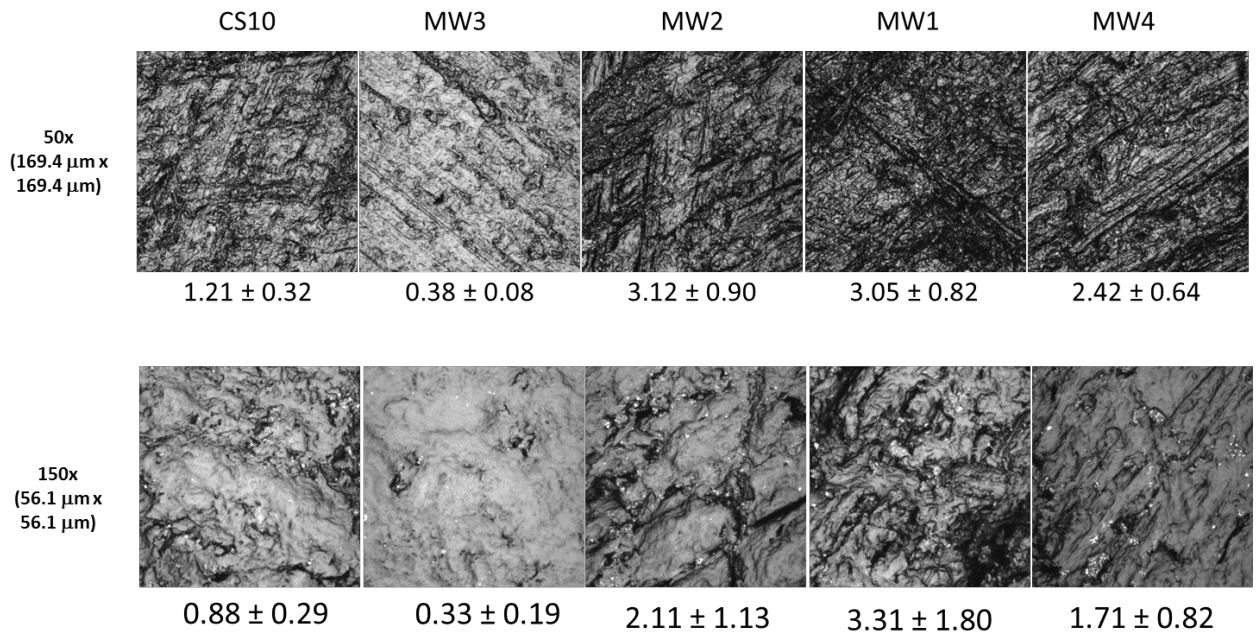

Figure 17. LSCM images taken at 50 x and 150 x magnifications on dry abraded NP surfaces by five different wheels. Abrasion was performed using the following parameters; speed: 6.28 rad/s (60 rpm), applied force: 1000 g, # of cycles: 100. RMS surface roughness values, in µm, are also included below each image for comparison. The results are the average of 8 measurements from 4 duplicates, and the ± values represent one standard deviation.

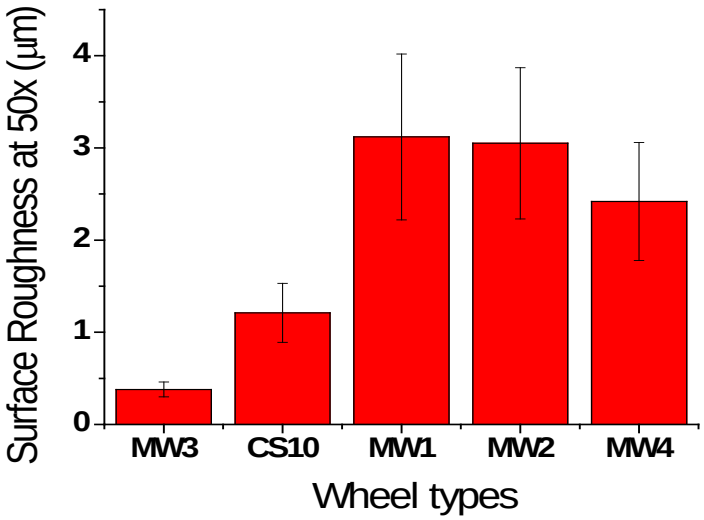

Figure 18. Surface roughness of dry abraded NC by five wheels. The results are the average of 8 measurements, and the error bars represent one standard deviation.

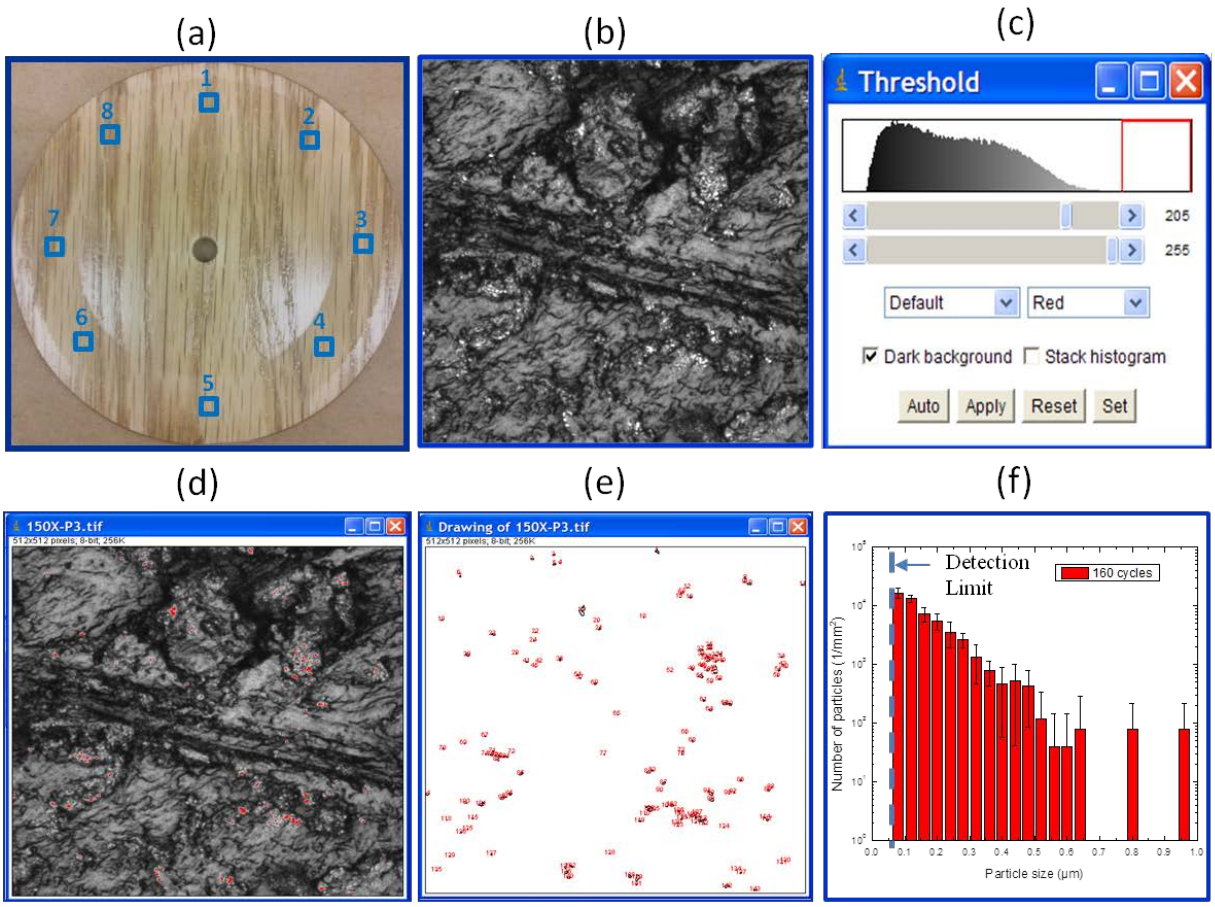

Figure 19. An example of using image analysis in LSCM to obtain the number and size distribution of surface release particles generated by abrasion of NC or NP. Error bars in (f) represent one standard deviation from the average of 8 measurements from 4 duplicates. The dashed line in (f) represents the detection limit for this LSCM method as described in the text.

To provide quantitative data on the number and size distributions of the surface release particles per unit abraded area, image analysis was performed on the LSCM images. By carefully adjusting the gray level, the number and size distribution of particles in the 56 µm x 56 µm abraded area from each 150 x LSCM image can be obtained. An example is displayed in Figure 19. Figure 19a is a picture of an abraded specimen showing the 8 different positions where the LSCM images were taken for analysis, Figure 19b is a 150x LSCM image of the abraded surface, Figure 19c is the gray level threshold setting, Figure 19d is the highlighted particles within the image as defined by the gray level threshold, Figure 19e is the particle counting numbers which tally the number of particles for each particle size, and Figure 19f is a bar plot of the total particles for each size from 0.08 µm to 1 µm. Note that LSCM, in

combination with image analysis, is a good and relatively fast method for quantifying the number and size distribution of released particles accumulated on abraded surfaces having particle sizes greater than 80 nm.

However, LSCM has its detection limit, and therefore cannot actually measure nanoparticles having particle sizes less than 80 nm. For particle sizes smaller than 80 nm, based on the SEM/TEM microscopic data from Year 1 research [30] and other previous studies [21, 23, 25, 28, 29], there is little evidence of free nanoparticles are released. The particles released during abrasion of polymer coatings and paints contain nanoparticles embedded in the polymer matrix. The size distribution in previous studies of airborne particles emitted by Taber abraser for polymer nanocomposites containing nanoZnO [23], nanoTiO_2 [25], and MWCNT [21] include particle sizes ranging from 0.1 μm to 50 μm.

The effects of wheel type on the number and size distribution of surface release particles for NC are illustrated in Figures 20 and 21. Note that the number of particles on the vertical axis is expressed with a logarithmic scale and all results are normalized to a 1 mm^2 abraded area. All abrasion operations were conducted in dry condition at 6.28 rad/s (60 rpm) speed, 1000 g applied force, and 100 cycles. Figure 20 displays the number and size distributions of released particles that stayed on specimen surface of the dry abraded NC samples using each of the five wheels. The surface characteristics from the abraded surfaces by each wheel are repesentative (as shown in Figure 17) and the results are the averages of 8 measurements from 4 duplicates. The majority of the surface release particles had a size ranging from 0.08 μm to 0.6 μm, with (95 ± 1) % falling between 0.08 μm and 0.3 μm. Figure 20 shows that, with a few exceptions, the number of surface release particles decreased with increasing size, with the largest amount for 0.08 μm and the smallest for (0.6 to 0.9) μm. Note that the particles generated in the abrasion process include particles on the coatings/paints surfaces, on the abrader, and particles may be dispersed into the air. However, the number of particles were presented here may not account for all the particles generated during the abrasion, but it is close enough for the assessment of particle release purpose, because the number of particles outside the abraded band is much smaller (almost zero) compared to those found in the abraded band area, as seen in the first year study [30] and very few airborne particles were detected as described in the separated reported [31].

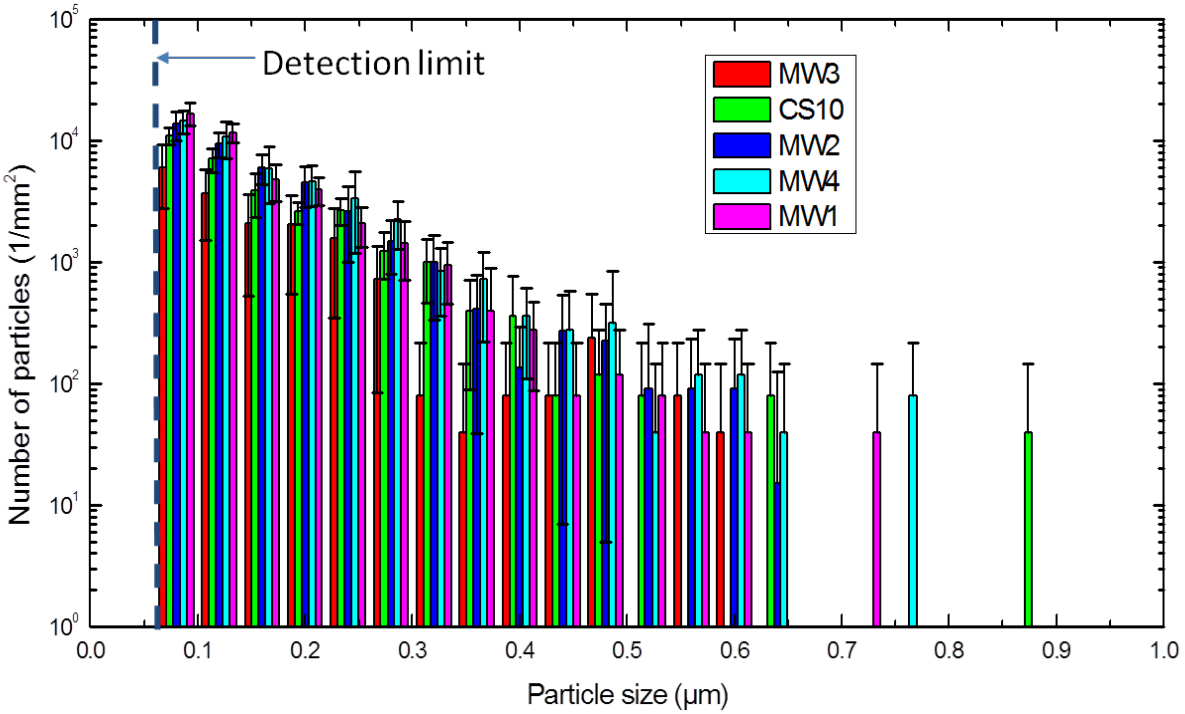

Figure 20. Number and size distributions of surface release particles of nanocoating abraded by five wheels. Abrasion was performed under dry condition at 6.28 rad/s (60 rpm), 1000g applied load, and 100 cycles. The results are the average of 8 measurements, and the error bars represent one standard deviation. The dashed line represents the detection limit for this LSCM method as described in the text.

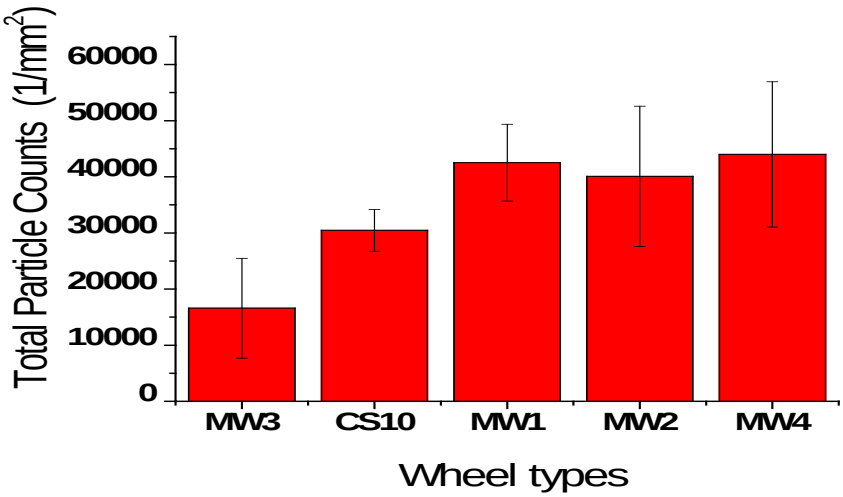

Figure 21. Total surface release particles per 1 mm^2 abraded area of NC for the five wheels. Abrasion was performed under dry condition at 6.28 rad/s (60 rpm), 1000 g load, and 100 cycles. The results are the average of 8 measurements, and the error bars represent one standard deviation.

As seen in Figure 21, MW1, MW2, and MW4 generated essentially the same total number of surface release particles for NC, while the smooth wheel (MW3) produced the least amount. Further, a substantial amount of particles released by abrasion of NC stayed on the abraded surfaces. These results indicated that the number of surface release particles depends strongly on the type of abrasive wheel. Among the five wheels, the smoother of the two wheels, MW3 and CS10, produced a lower number of surface release particles than the other three wheels; the smoothest wheel (MW3) generating the least number of surface release particles (only 1/3 of the amounts from MW4).

The results of Figures 20 and 21 are summarized in Table 2. The value at the bottom of each column is the coefficient of variation (100 x standard deviation/mean). It is interesting to observe that the smoothest wheel MW3 yielded the highest coefficient of variation (least reproducible). Further, MW2 and MW4 also produced relatively high coefficients of variation. Undoubtedly, the abraded surface features, the gray level threshold selection, and the variability of particle distribution on the surface during the repeated abrasion may contribute to the high standard deviation values. It is also noted that surface release particles tend to accumulate on the edge of the circular abraded ring, and that the release particles redistribute on the abraded surfaces after each cycle. Therefore, investigation of the profile/surface roughness of the wheel(s) and abrasion parameters (# of cycles, loads) are needed to generate reproducible release of particles from NC by abrasion.

For the wet abrasion study, fewer abrasion cycles on the order of 100 or less are expected to generate similar results to those seen with dry abrasion. To achieve better statistics for released particles and mass loss analyses, a wheel that generates a higher number of released particles is better. In this case, MW2 and MW4 were chosen for the following abrasion study in wet conditions. MW3 was no longer available because MW3 wheel was used to make the MW4 (sand blasted). MW1 was not selected because 1) MW1 was made of corroded stainless steel, and 2) MW1 and MW4 have a similar roughness and surface patterns. For future study and standardization of the abrasion wheels, new versions of the MW3, MW2, and MW4 wheels can be fabricated with different degrees of abrasion resistance (mild, harsh, severe) for specific surface patterns and roughness levels for nanoparticle release from different polymer composites.

Table 2. Number and size distributions of surface release particles for dry abraded nanocoating by five wheels; abrasion parameters: speed: 60 rpm (6.28 rad/s), applied force: 1000 g, number of cycles: 100, for five different wheels. The results are the average of 8 measurements (from 4 duplicates). The % value at the bottom of each column is the coefficient of variation (100 x standard deviation/mean).

Particle Size (μm)	**MW3**	**CS10**	**MW1**	**MW2**	**MW4**
0.08	5 956	10 958	16 676	13 658	14 412
0.12	3 653	7 028	11 633	9 483	10 641
0.16	2 065	3 851	4 764	6 035	5 916
0.2	2 025	2 581	3 931	4 492	4 566
0.24	1 548	2 660	2 065	2 586	3 335
0.28	715	1 231	1 429	1 497	2 223
0.32	79[#]	993	953	998	834
0.36	40	397	397	408	715
0.4	79	357	278	136	357
0.44	79	79	79	272	278
0.48	238	119	119	227	318
0.52	0	79	79	91	40
0.56	79	0	40	91	119
0.6	40	0	40	91	119
> 0.6	0	119	40	15	119
Total surface particle ($1/mm^2$)	16 596 ± 53.6%	30 452 ± 12.2%	42 523 ± 16.1%	40 080 ± 31.2%	43 992 ± 29.4%

[#] *The repeating numbers, such as 40, 79, 91 and 119, would be artifacts from the image analyses, further investigations are needed to eliminate these artifacts.*

3.2.2. Effects of Wheel Type on Surface Release Particles by Abrasion in Liquid

Figure 22 displays representative LSCM images obtained at two different magnifications for NC surfaces abraded using two different metallic wheels, MW2 and MW4 (for surface profile and roughness of these two wheels, see Figure 4). These images were obtained from specimens from wet abrasion at 6.28 rad/s (60 rpm), 1000 g load, and 100 cycles. As indicated earlier, the bright dots observed in a LSCM image are the loose particles generated by the abrasion, i.e., surface release particles.

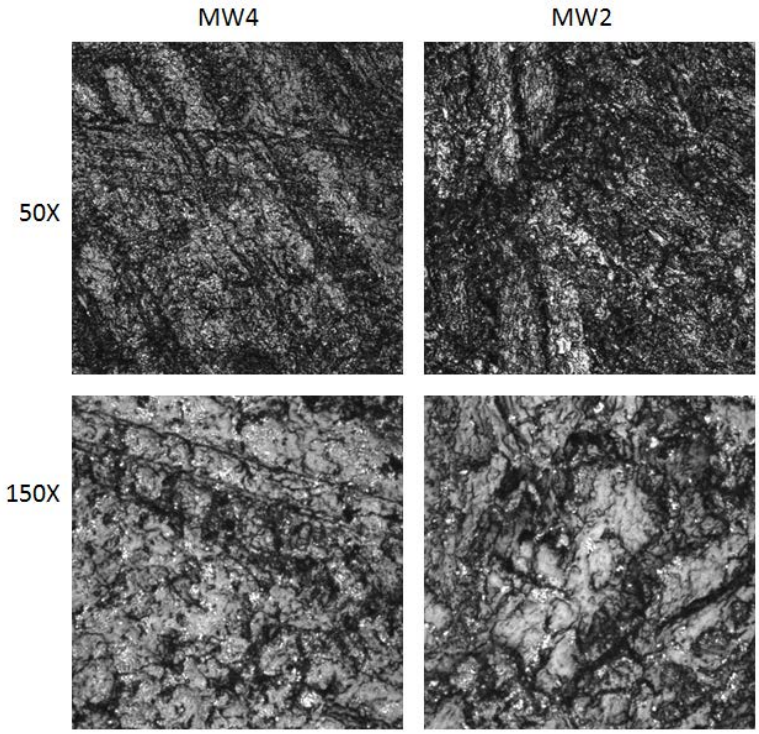

Figure 22. LSCM images taken at two magnifications for wet abrasion of NC using two different metallic wheels (MW4 and MW2). Abrasion parameters; speed: 6.28 rad/s (60 rpm); applied force: 1000 g, and number of cycles: 100.

By using the image analysis technique, similar to that illustrated in Figure 19, the number and size distributions of these loose particles that stayed on the specimen surface after wet abrasion of NC for the two metallic wheels were obtained, and the results are summarized in Table 3. All results are the average of 8 images from 4 duplicates. The MW4 wheel released more particles in all sizes than the MW2 wheel and 40 % to 50 % more for particle sizes $< 2.0\ \mu m$. For both wheels, the results show that the majority of particle sizes generated by wet

abrasion were between 0.08 µm and 0.3 µm, similar to that observed for dry abrasion. However, under the same parameters and for all particle sizes, wet abrasion yielded substantially more surface release particles than those from dry abrasion (compare Tables 2 and 3, 43 992 ± 29.4 % vs 120 621 ± 23.7 %). Table 3 also reveals that the coefficients of variation for surface release particles by wet abrasion appear to be lower than those by dry abrasion.

Table 3. Number and size distribution of surface release particles for wet abrasin of NC using two metallic wheels; all abrasions were performed at 6.28 rad/s (60 rpm), 1000 g applied force, and 100 cycles. All results are the average of 8 measurements (from 4 duplicates). The % value at the bottom of each column is the coefficient of variation (100 x standard deviation/mean)

Particle size (µm)	**MW2**	**MW4**
0.08	27 872	43 952
0.12	22 988	32 557
0.16	11 832	16 001
0.2	7 385	12 507
0.24	5 281	6 988
0.28	3 017	3 732
0.32	1 707	1 945
0.36	1 271	1 231
0.4	993	794
0.44	238	397
0.48	476	40
0.52	278	159
0.56	318	159
0.6	40	79
> 0.6	239	80
Total surface particles ($1/mm^2$)	83 935 ± 24.8 %	120 621 ± 23.7 %

3.3. Effect of Abrasion Cycle on Particle Release – Dry Abrasion

3.3.1. Nanocoating (NC)

As mentioned in last section MW2 and MW4 are both suitable for dry and wet abrasion studies, with MW4 generating more released particles. However, MW4 was made by sand blasting techniques with a random surface pattern and fabricated at later time. There were not enough samples to repeat all the measurements already done using MW2 wheel. Furthermore, the results using MW4 wheel should be expected to be better (more released particles, better statistics) to those using MW2. For future standardization of the abrasion wheels for nanoparticle release, MW2 is selected for the dry and wet abrasion experiments of NC and NP. Figure 23 displays pictures and representative LSCM images at two magnifications of dry abraded NC for four different numbers of cycles. All abrasions were performed at 6.28 rad/s (60 rpm) and 1000 g applied force using the MW2 wheel. At low magnification LSCM (middle row), the surface of the NC shows heterogeneous features consisting of dark and bright regions, reflecting a difference in surface topography of the specimen. Based on the results for both 50 x and 150 x LSCM images, the abrasion cycle had little effect on the surface roughness abraded by the MW2 wheel. The surface roughness values were similar. Roughness values of the abraded specimens obtained from the 50x images were between (1.85 ± 0.54) µm and (2.29 ± 0.72) µm and the values taken from the 150x images ranged from (1.33 ± 0.48) µm and (1.62 ± 0.97) µm, respectively.

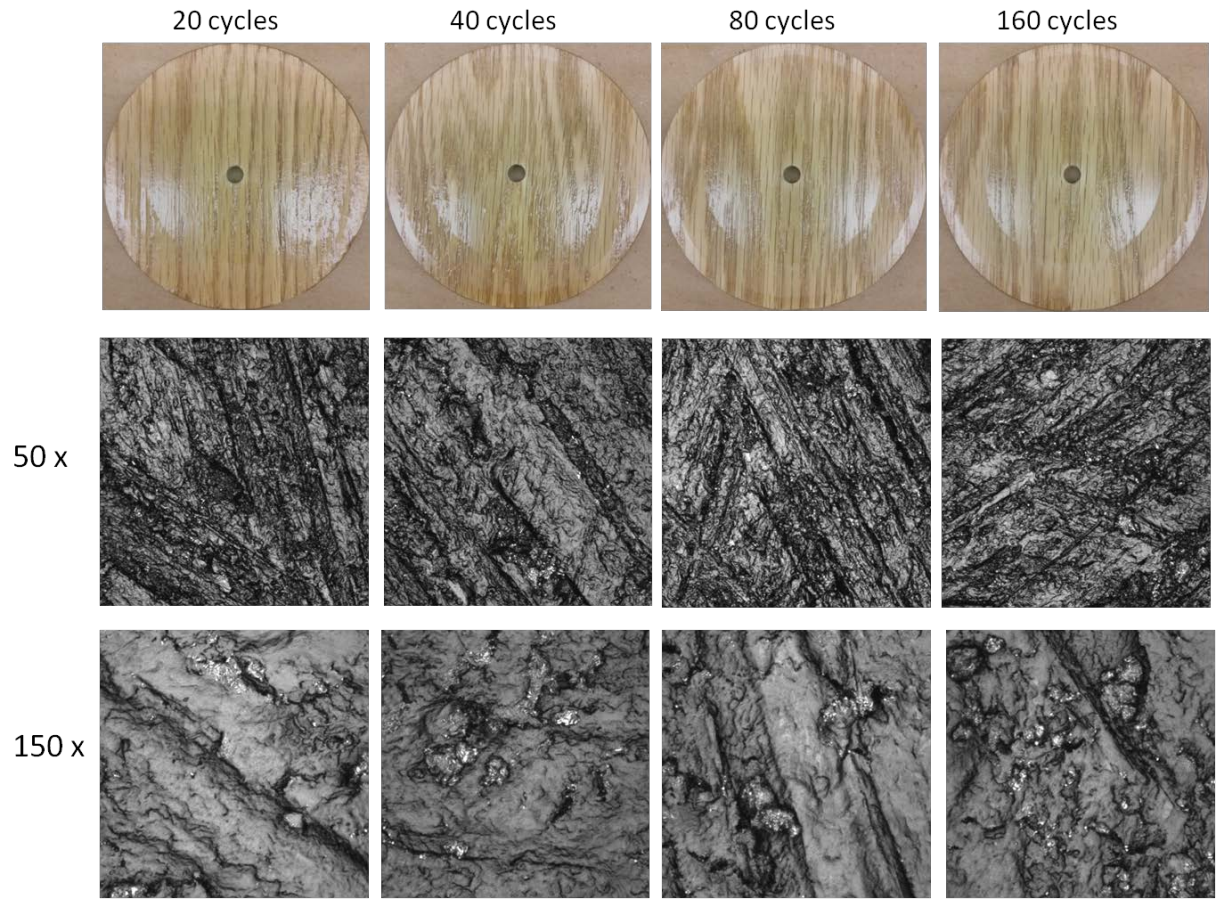

Figure 23. Pictures (top) and LSCM images at two magnications (middle and bottom rows) of dry abraded nanocoating at four different cycles using MW2 wheel; abrasion at 6.28 rad/s (60 rpm) and a 1000 g applied force.

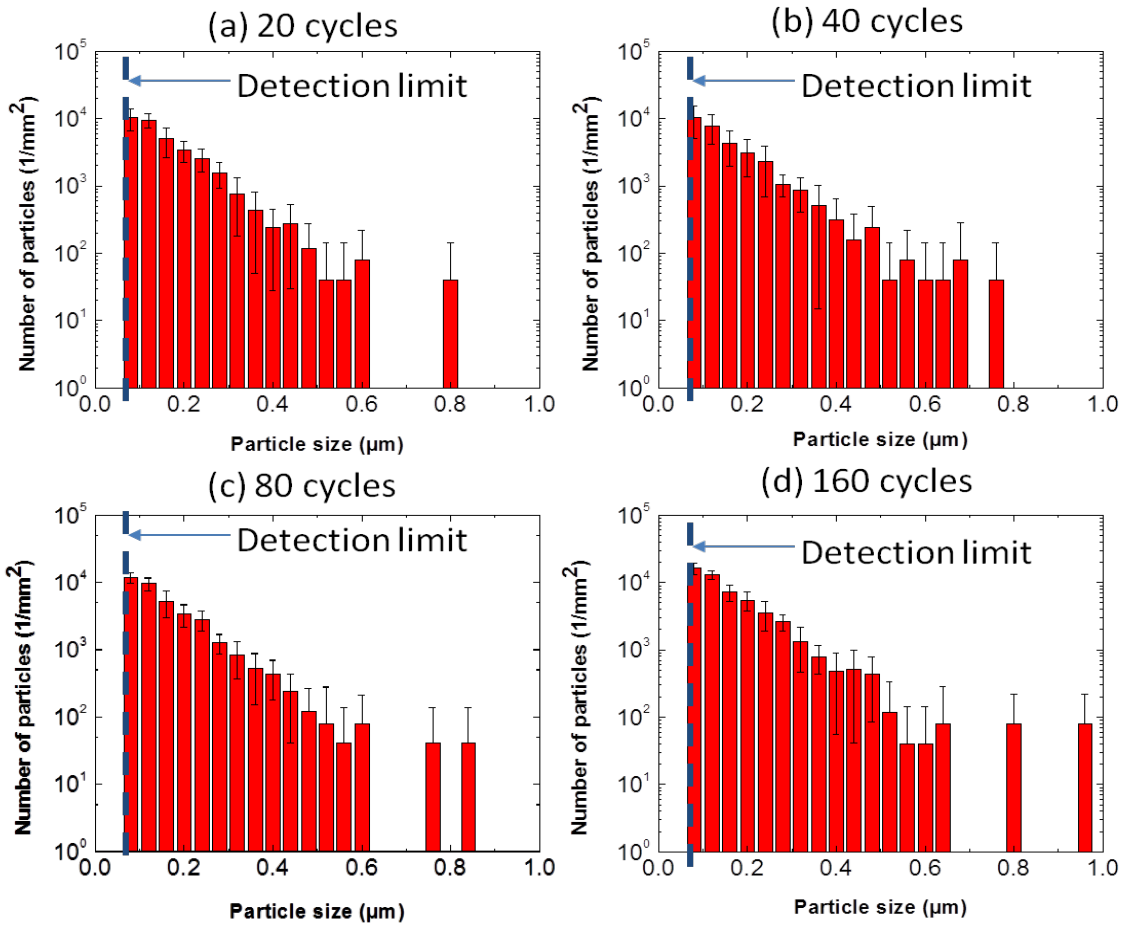

Figure 24. Size and number of surface release particles for four different abrasion cycles as indicated in the graphs for dry abraded NC at 6.28 rad/s (60 rpm) and 1000 g applied force using the MW2 wheel. The results are the average of 8 measurements (from 4 duplicates), and the error bars represent one standard deviation. The dashed lines represent the detection limit for this LSCM method as described in the text.

The effects of the number of abrasion cycles on the number and size distributions of surface release particles of NC are presented in Figure 24 and summarized in Table 4. The data for each abrasion cycle were obtained from LSCM images taken from 8 different locations of the abraded specimens. In addition to number and size distributions of surface release particles, Table 4 also included the mass loss as a function of abrasion cycles. The relative mass loss, in %, was determined as the difference in mass of the specimen before and after abrasion divided by the mass of the NC within the circular abraded area multiplied by 100. The mass of the NC within the abraded area was calculated based on a surface area of 30 cm^2 (12.5 mm width) and a thickness of 256 μm ± 16 μm, and a NC density of 1.15 g/cm^3 as given in Table 1.

Table 4 shows that the surface release particles generated from NC for all four cycles had a size ranging from 0.08 µm to 0.6 µm, with slightly higher than 50 % falling between 0.08 µm and 0.12 µm. Further, the number of surface release particles generally increased as particle size decreased, similar to earlier results on the wheel type effect. The total number counts between 20 cycles and 80 cycles were similar within experimental uncertainties, as shown in Figure 25a, while the total number of surface release at 160 cycles had the highest. The mass data showed that little difference exhibited between 20 cycles and 40 cycles, but substantially higher mass loss at 160 cycles (Figure 25b). The small effect of the number of cycles between 20 and 40 on surface release particles may be due to the sample roughness and the distribution of particles in the coatings is not uniform. Early cycles (< 40) of abrasion mostly take out the peak (hills) areas above the averaged plane surface, while later cycles (> 80) remove the entire surface area. Therefore, the selection of a proper cycle for studying the abrasion of coatings or paints may depend on the surface roughness of the material. If the surface is relatively smooth, a smaller number of cycles may be adequate; but if the surface is relatively rough, a larger number of cycles may be required. Of course, the force applied during abrasion and the surface profile of the wheel also plays an important in the quantity of material removed by abrasion.

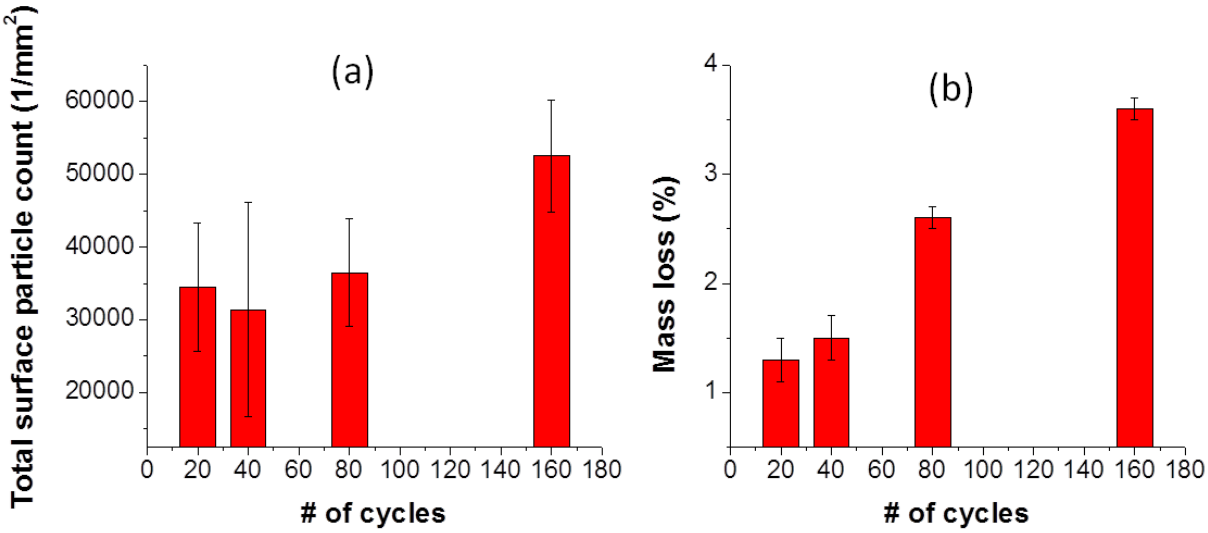

Figure 25. (a). The total surface particle counts, (b) mass loss for four different abrasion cycles of the NC dry abrasion results. Abrasion parameters: 6.28 rad/s (60 rpm) and 1000 g applied force. The results are the average of 8 measurements for (a) particle count and the average of 3 measurements for (b) mass loss, and the error bars represent one standard deviation.

Table 4. Effects of abrasion cycle on the number and size distribution of surface release particles and mass loss of dry abraded NC using MW2 wheel; abrasion at 6.28 rad/s (60 rpm) and a 1000 g applied force. The results are the average of 8 measurements from 4 duplicates for particle count and the average of 3 measurements for mass loss. The % value at the bottom of each column is the coefficient of variation (100 x standard deviation/mean).

Particle Size(μm)	**20 cycles**	**40 cycles**	**80 cycles**	**160 cycles**
0.08	10 283	10 283	11 752	16 398
0.12	9 529	7 861	9 529	13 221
0.16	5 003	4 288	5 241	7 226
0.2	3 454	3 137	3 415	5 479
0.24	2 581	2 303	2 819	3 573
0.28	1 588	1 072	1 270	2 620
0.32	754	873	834	1 310
0.36	437	516	516	794
0.4	238	318	437	476
0.44	278	159	238	516
0.48	119	238	119	437
0.52	40[#]	40	79	119
0.56	40	79	40	40
0.6	79	40	79	40
> 0.6	40	159	80	228
Total surface particles ($1/mm^2$)	34 463 ± 25.7 %	31 366 ± 46.9 %	36 448 ± 20.4 %	52 486 ± 14.7 %
Mass loss (%)	1.3 ± 0.2	1.5 ± 0.2	2.6 ± 0.1	3.6 ± 0.1

[#] *The repeating numbers, such as 40, 79, 91 and 119, would be artifacts from the image analyses, further investigations are needed to eliminate these artifacts.*

3.3.2. Nanopaint (NP)

Figure 26 presents pictures and representative LSCM images at two magnifications of NP abraded under dry condition for four different numbers of cycles. All abrasions were done at 6.28 rad/s (60 rpm) and 1000 g applied force using the MW2 wheel. The removal of NP by dry abrasion was visible by the naked eye for all four cycles. The roughness values of the abraded specimens obtained from the 50x images were between 1.43 µm and 2.83 µm and those measured from the 150x micrographs ranged from 1.1 µm and 2.42 µm. There is no significant difference between the RMS roughness values of 20 cycles and 40 cycles due to large experimental uncertainties. The RMS values of 80 cycles and 160 cycles are smaller than those of lower abrasion cycles.

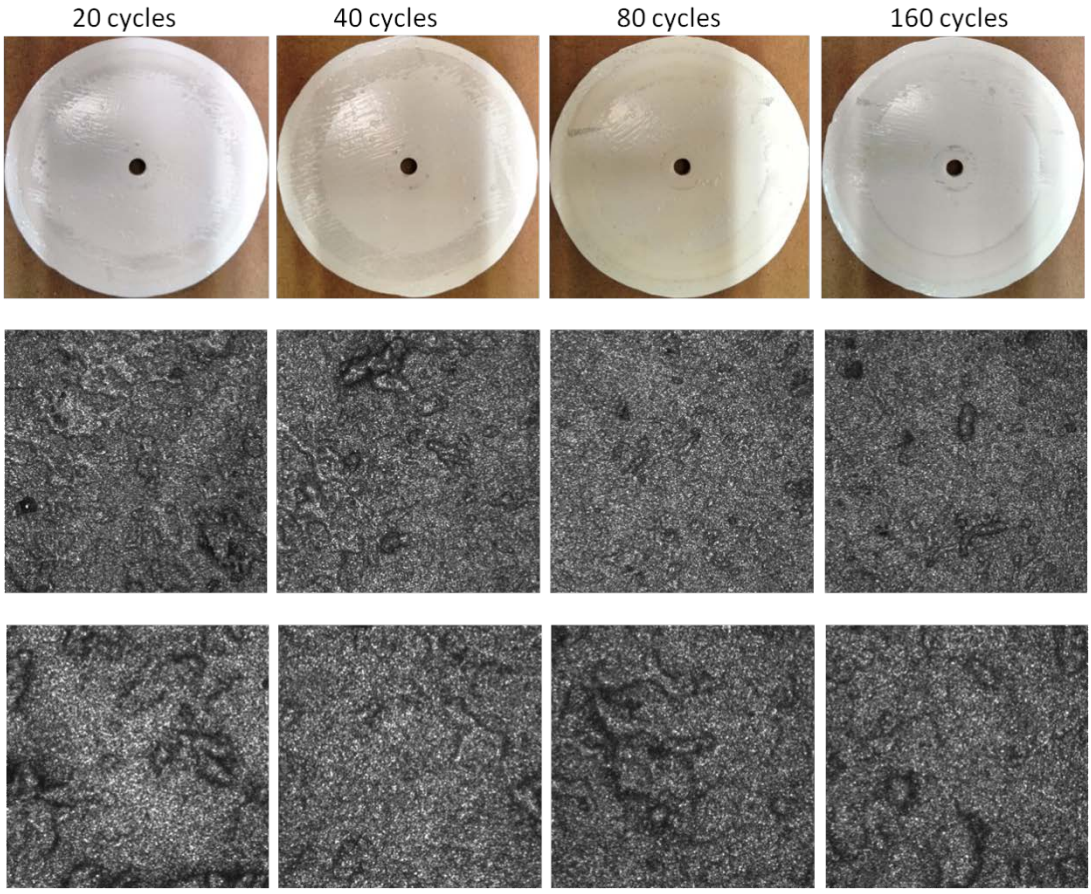

Figure 26. Pictures (top) and LSCM images at two magnications (middle and bottom rows) of the abraded nanopaint at four different cycles using MW2 wheel; abrasion at 60 rpm and a 1000g applied force.

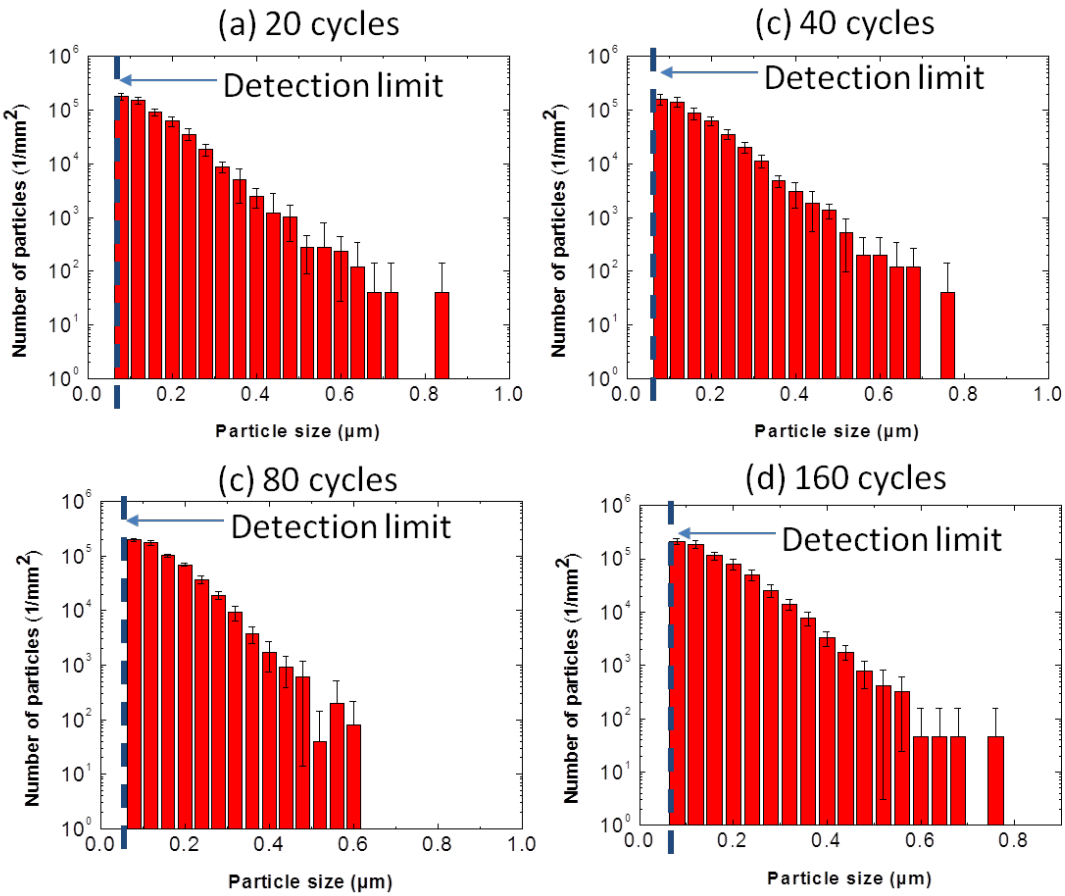

Figure 27. Size and number of surface release particles for four different abrasion cycles as indicated in the graphs for dry abraded NP at 6.28 rad/s (60 rpm) and 1000 g applied force using the MW2 wheel. The results are the average of 8 measurements (from 4 duplicates), and the error bars represent one standard deviation. The dashed lines represent the detection limit for this LSCM method as described in the text.

The effects of abrasion cycles on the number and size distributions of surface release particles on NP are presented in Figure 27 and summarized in Table 5. The data for each abrasion cycle were obtained from the 150x LSCM images taken from 8 different locations of the abraded specimens, similar to that for NC. In addition to the number and size distributions of surface release particles, Table 5 also included the mass loss as a function of abrasion cycles of NP. The relative mass loss was determined by the same method for NC using the thickness and density values of NP given in Table 1. Table 5 (and Figure 28) reveals that, except for the 20 cycles and 40 cycles, which exhibited little effect, 80 cycles and 160 cycles produced higher total surface release particles as well as higher number of particles for each size between 0.08 μm and 0.2 μm. Similar to the results for the NC samples, the size of surface release particles from NP

abraded at different cycles ranged from 0.08 µm to 0.6 µm, with a majority of them between 0.08 µm and 0.3 µm. Further, the number of surface release particles decreased with increasing particle size. Figure 28 shows the plots of (a) total surface release particle count (b) mass loss data for four different cycles. The total surface release particle counts at 20 cycles and 40 cycles (even at 80 cycles) are not significantly different, but these results of the mass loss data show substantially higher mass losses at 80 cycles and 160 cycles, with the highest cycle lost the most mass, similar to that for NC. Note that the mass loss in Figure 28b includes not only the released particles but also NC polymer blinders. The total surface release particle counts in Figure 28a reflect what was observed on the abraded surface. Therefore, there is no direct correlation between the total surface release particle counts and the mass loss at any abrasion conditions.

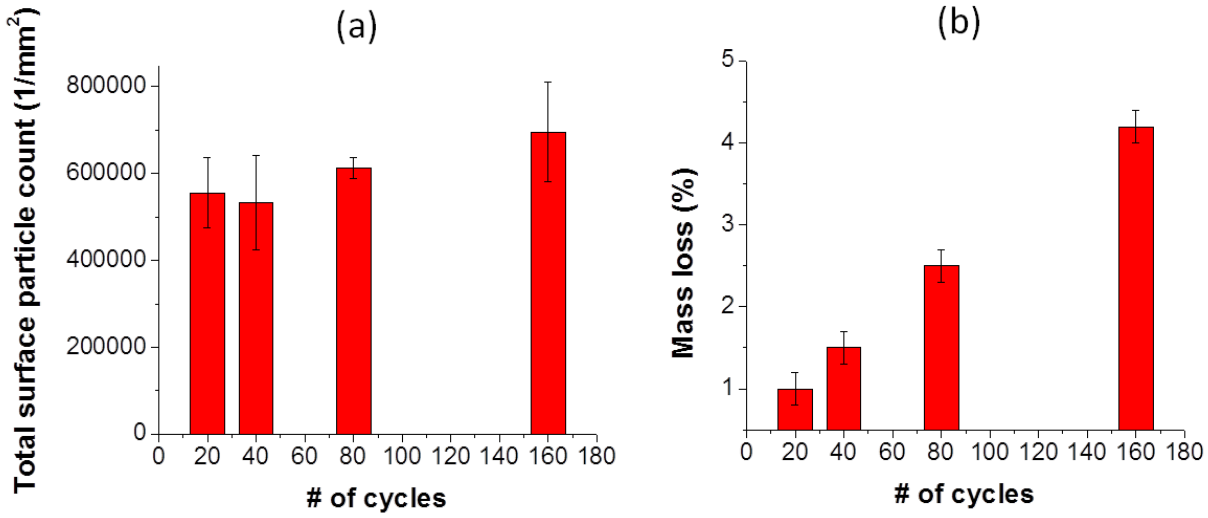

Figure 28. (a). The total surface released particle counts, (b) mass loss for four different abrasion cycles of the NP dry abrasion results. Abrasion parameters: 6.28 rad/s (60 rpm) and 1000 g applied force. The results are the average of 8 measurements for (a) particle count and the average of 3 measurements for (b) mass loss, and the error bars represent one standard deviation.

One interesting result is that, despite similar mass losses due to dry abrasion between NP and NC, the numbers of particles stayed on the abraded NP surface for all cycles were more than one order of magnitude greater than those on abraded NC surface. The exact reason for this difference is unknown. One reason may be due to the difference in mechanical properties of the two materials. NP is softer, has a much lower modulus, and has a rubbery behavior with higher elongation at break as compared to the more rigid, shorter elongation at break NC (from Figure 7a). Probably it is more difficult for the softer and rubbery NP release particles to fly off

the surfaces during abrasion (i.e., more released particles stay on the abraded surface) than the harder and more rigid NC release particles. This explanation is partially supported by the coefficients of variation, which are lower for the rubbery NP than for the more rigid NC (compare Tables 4 and 5).

Table 5. Effects of abrasion cycle on the number and size distribution of surface release particles and mass loss of dry abraded NP using the MW2 wheel. Abrasion parameters; speed: 6.28 rad/s (60 rpm), applied force: 1000 g. The results are the average of 8 measurements from 4 duplicates for particle count and the average of 3 measurements for mass loss. The % value at the bottom of each column is the coefficient of variation (100 x standard deviation/mean).

Particle Size (µm)	**20 cycles**	**40 cycles**	**80 cycles**	**160 cycles**
0.08	177 435	159 807	197 009	211 251
0.12	152 263	143 449	173 147	187 308
0.16	91 080	87 467	101 125	114 570
0.2	61 818	63 168	69 084	79 930
0.24	35 574	35 455	37 083	49 569
0.28	18 422	20 328	19 018	25 172
0.32	8 735	11 316	9 330	13 929
0.36	4 963	4 804	3 732	7 693
0.4	2 501	3 017	1 707	3 323
0.44	1 191	1 826	913	1 775
0.48	1 032	1 350	596	774
0.52	278	516	40	410
0.56	278	199	199	319
0.6	238	199	79	46
> 0.6	239	278	0	138
Total surface particles ($1/mm^2$)	556 047 ± 14.6 %	533 179 ± 20.5 %	613 062 ± 3.9 %	696 207 ± 16.6 %
Mass loss (%)	1.0 ± 0.2	1.5 ± 0.2	2.5 ± 0.2	4.2 ± 0.2

3.4. Effect of Abrasion Cycle on Particle Release – Wet Abrasion

3.4.1. Nanocoating (NC)

Figure 29 displays pictures and representative LSCM images at two magnifications for wet abrasion of NC at four different numbers of cycles. All abrasions were performed at 60 rpm and 1000g applied force using the MW2 wheel. The circular abraded band is visible for all cycles, which is different for dry abrasion where the abraded zone is clearly visible only at 40 cycles or greater. The RMS roughness of the abraded specimens obtained from the 50x images varied between 3.45 µm and 7.37 µm and that taken from the 150x micrographs ranged from 2.45 µm and 4.49 µm. The RMS roughness results indicate that abrasion cycle had only a small effect on surface roughness of wet abraded NC with the MW2 wheel. These values are respectively greater than those obtained from dry abraded specimens, which ranged from 1.84 µm to 2.29 µm for 50x images and between 1.33 µm and 1.62 µm for 150x micrographs. These results suggest that the surface of wet abraded NC is rougher than that of dry abraded sample.

The number and size distributions of surface release particles as a function of cycles for wet abraded NC are summarized in Table 6. In addition to number and size distributions of surface release particles, Table 6 also included the mass loss as a function of abrasion cycles. The relative mass loss, expressed as a percentage, was determined by first measuring the dry mass of particles released in water, as described in the experimental section. This release particle mass was then divided by the mass of the NC within the circular abraded area multiplied by 100. The mass of the NC within the abraded area was obtained similarly to that for dry abraded NC using the same density and thickness values given in Table 1. In this way, the mass loss values measured during dry abrasion (obtained from the specimen before and after abrasion) can be compared directly with the mass loss (obtained by measuring the released particles) due to wet abrasion. This comparison will be presented later.

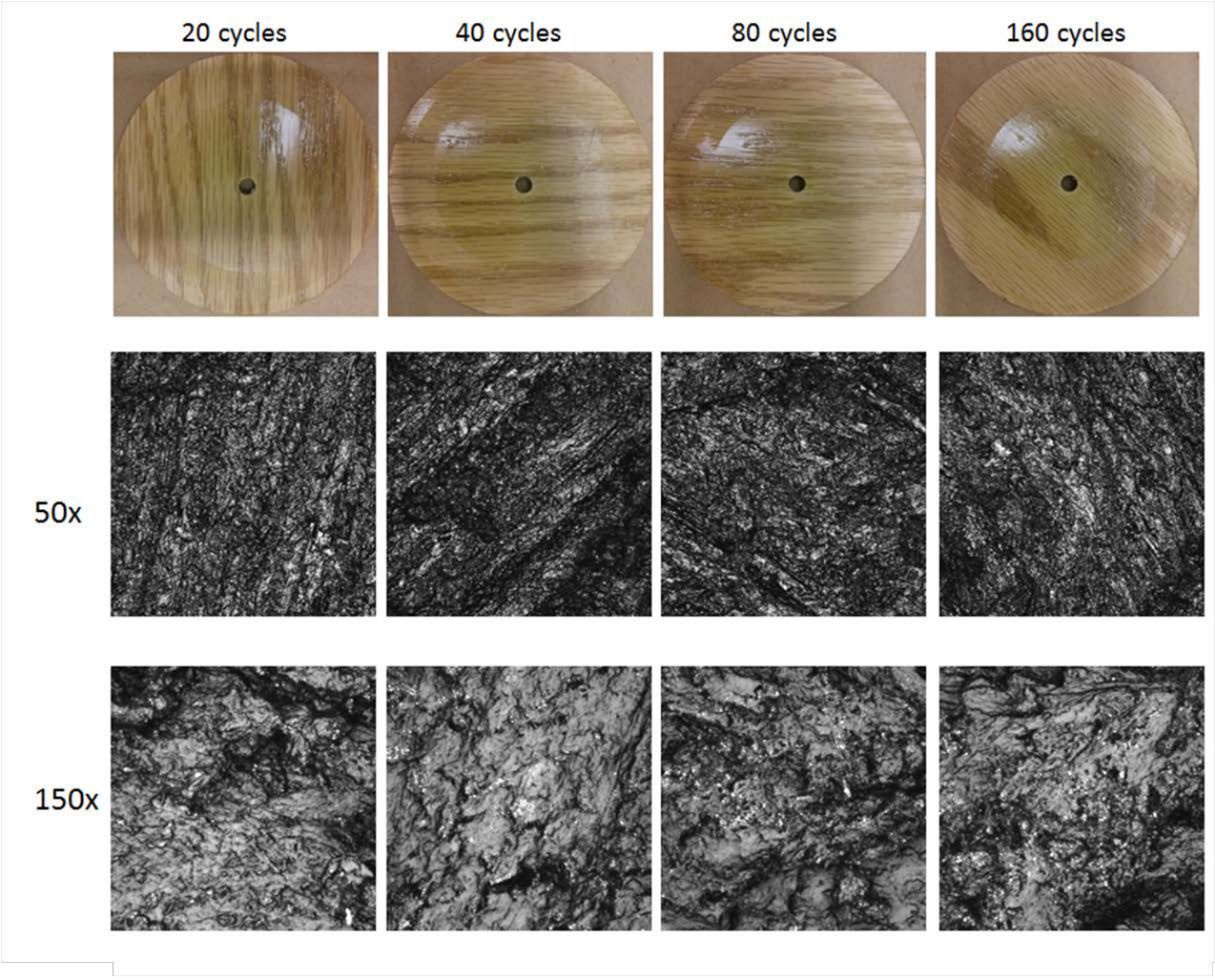

Figure 29. Pictures (top) and LSCM images at two magnications (middle and bottom rows) for wet abraded nanocoating at four different cycles using MW2 wheel; abrasion at 6.28 rad/s (60 rpm) and a 1000 g applied force.

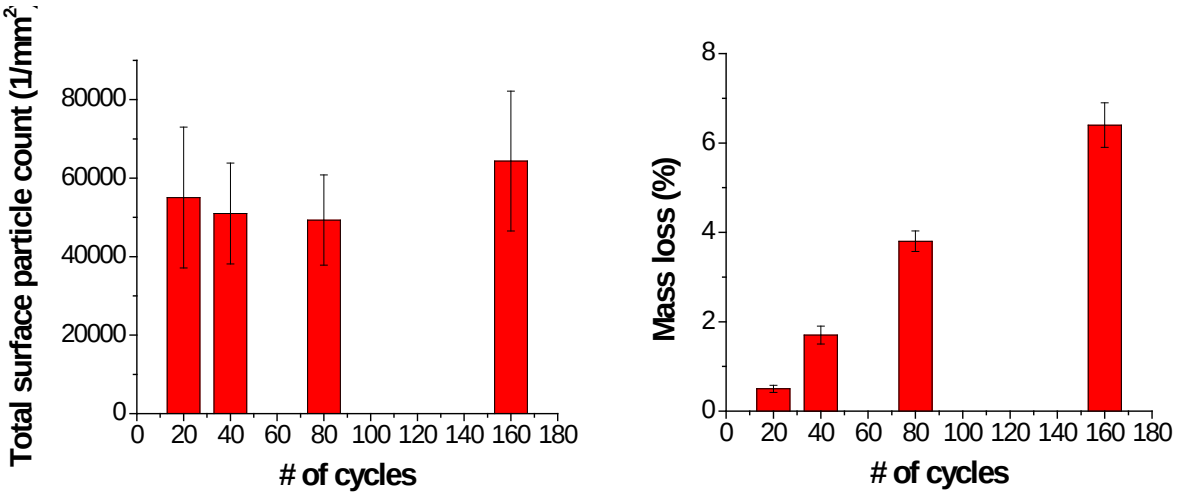

Figure 30. (a) The total surface particle counts, (b) mass loss for four different abrasion cycles of the NC wet abrasion results. Abrasion parameters: 6.28 rad/s (60 rpm) and 1000 g applied force. The results are the average of 8 measurements for (a) particle count and the average of 3 measurements for (b) mass loss, and the error bars represent one standard deviation.

Table 6 shows that most of surface release particles generated by wet abrasion of NC for all number of cycles fell between 0.08 µm and 0.3 µm, similar to those for NC and NP abraded under dry condition. There is no strong effect of the number of cycles on the the total surface release particle counts, as shown Figure 31a. The total particle count was slightly higher at 160 cycles than others. However, the mass loss data clearly showed a substantial increase with increasing number of cycles, from 0.5 % at 20 cycles to 6.4 % at 160 cycles. In addition, the number of surface release particles generated during abrasion for all cycles were substantially greater than those released by dry abrasion (compare Tables 4 and 6). Again, the mass loss in Figure 30b includes not only the released particles but also NC polymer binders. The total surface release particle counts in Figure 30a reflect what was observed on the abraded surface. Therefore, there is no direct correlation between the total surface release particle counts and the mass loss at any abrasion conditions.

Table 6. Effects of abrasion cycle on the number and size distribution of surface release particles and mass loss of wet abraded NC using the MW2 wheel. Abrasion parameters; speed: 6.28 rad/s (60 rpm), applied force: 1000 g. The results are the average of 8 measurements from 4 duplicates for particle count and the average of 3 measurements for mass loss. The % value at the bottom of each column is the coefficient of variation (100 x standard deviation/mean).

Particle Size (µm)	**20 cycles**	**40 cycles**	**80 cycles**	**160 cycles**
0.08	18 986	18 657	17 430	22 141
0.12	14 856	13 299	12 639	16 848
0.16	7 854	7 347	7 093	9 198
0.2	5 544	4 557	4 791	6 167
0.24	3 248	3 190	3 110	4 447
0.28	1 761	1 795	1760	2 541
0.32	1 112	925	926	1 178
0.36	520	525	543	596
0.4	361	193	371	463
0.44	144	249	212	291
0.48	188	69	106	212
0.52	144	41	159	79
0.56	101	0	66	53
0.6	29	28	26	40
> 0.6	200	97	91	79
Total surface particles ($1/mm^2$)	55 048 ± 32.6 %	50 972 ± 25.2 %	49 323 ± 23.3 %	64 346 ± 27.7 %
Mass loss (%)	0.5 ± 0.08	1.7 ± 0.2	3.8 ± 0.23	6.4 ± 0.5

3.4.2. Nanopaint (NP)

Pictures and representative LSCM images at two magnifications of NP surface after wet abrasion at four different cycles are displayed in Figure 31. All abrasions were performed at 6.28 rad/s (60 rpm) and 1000 g applied force using the MW2 wheel. The uniform circular abraded zones were clearly visible by the naked eye at all four cycles. There was no apparent trend on effect of cycle on surface roughness of wet abraded NP. The roughness of the abraded specimens obtained from the 50x images were between 3 µm and 5.4 µm. These values are greater than those obtained from images of same magnification for dry abraded NP (Figure 29), which ranged from 1.43 µm to 2.83 µm.

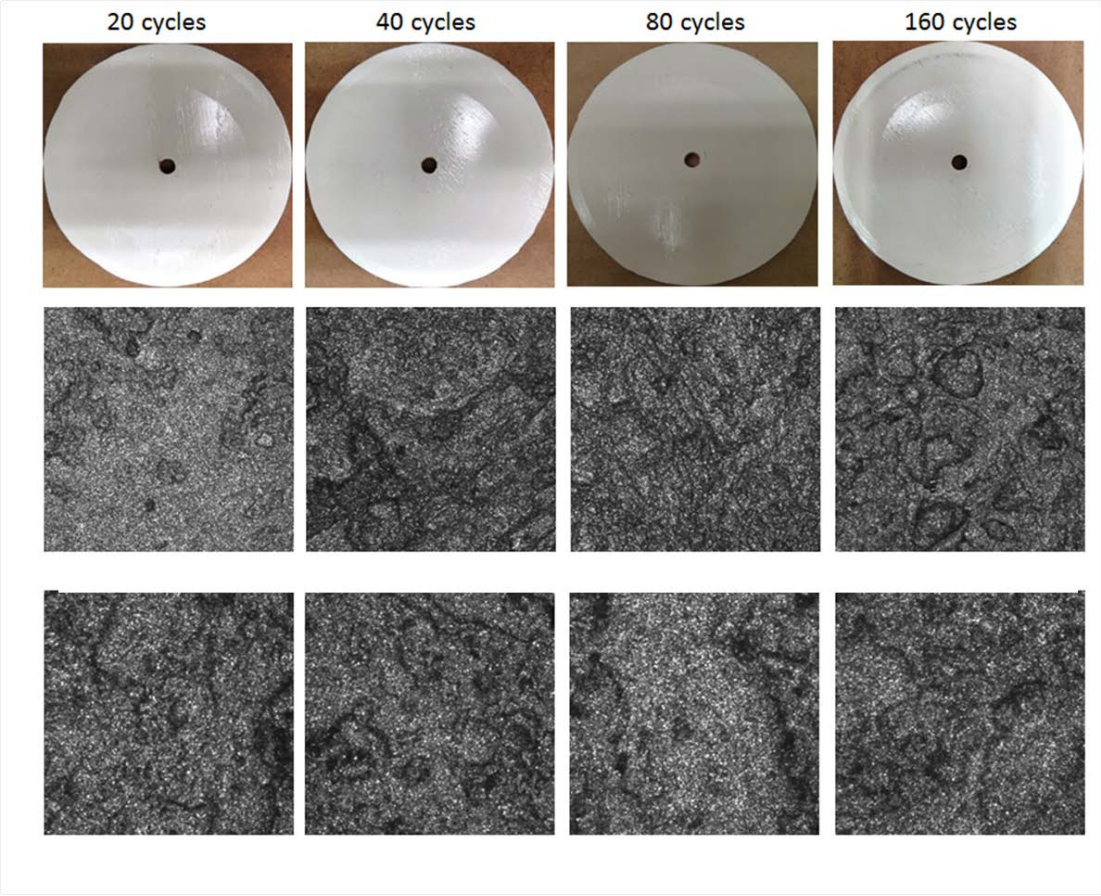

Figure 31. Pictures (top) and LSCM images at two magnications (middle and bottom rows) of wet abraded nanopaint at four different cycles using MW2 wheel; abrasion at 60 rpm and a 1000g applied force.

The effects of abrasion cycles on the number and size distributions of surface release particles of wet abraded NP samples are summarized in Table 7. The data for each abrasion cycle were obtained from the 150x LSCM images taken from 8 different locations of the abraded specimens, similar to that for NP samples. In addition to the number and size distributions of surface release particles, Table 7 also included the mass loss as a function of abrasion cycles of NP. The relative mass loss was determined by the same method used for the wet abraded NC based on the thickness and density values of NP given in Table 1.

Figure 32 displays (a) the total surface release particles on abraded surface and (b) mass loss for 4 different abrasion cycles. Figure 32a reveals that the number of cycles during wet abrasion essentially had no effect on the total surface released particles. These results of surface release particles are in contrast with the mass loss data, which clearly showed a linearly increase with increasing number of cycles, from 0.6 % at 20 cycles to 4.3 % at 160 cycles. From Table 7, most of surface released particles generated by wet abrasion of NP for all number of cycles fell between 0.08 μm and 0.2 μm, similar to that for wet and dry abraded NC. Comparing with the results in Table 5, the numbers of surface release particles during wet abrasion are quite similar to those of dry abrasion. A comparison of the mass loss for abrasion in these two media is presented later.

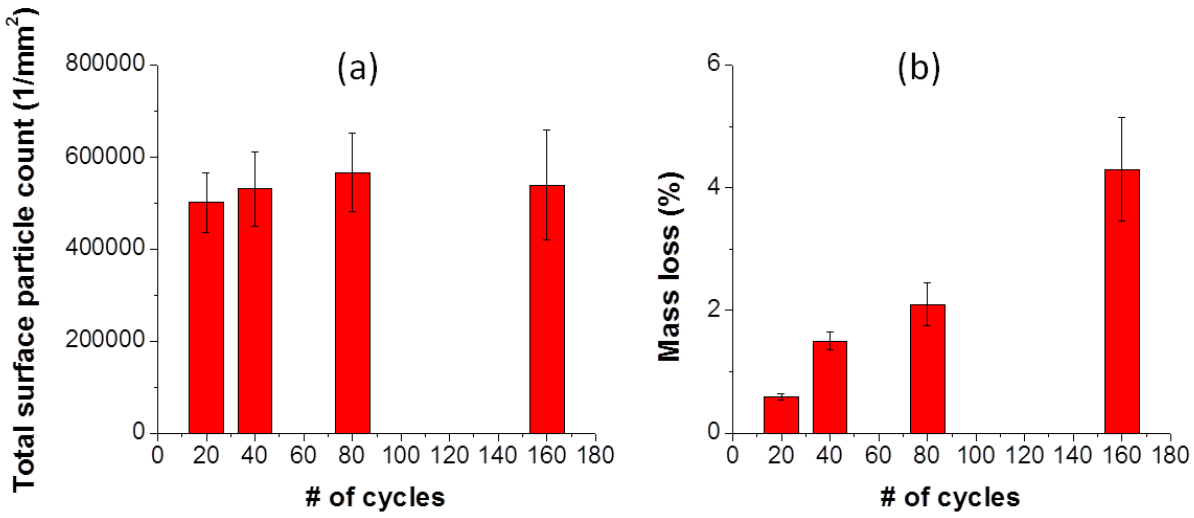

Figure 32. (a) The total surface particle counts, (b) mass loss for four different abrasion cycles of the NP wet abrasion results. Abrasion parameters: 6.28 rad/s (60 rpm) and 1000 g applied force. The results are the average of 8 measurements for (a) particle count and the average of 3 measurements for (b) mass loss, and the error bars represent one standard deviation.

Table 7. Effects of abrasion cycle on the number and size distribution of surface release particles and mass loss of wet abraded NP using the MW2 wheel. Abrasion parameters; speed: 6.28 rad/s (60 rpm), applied force: 1000 g. The results are the average of 8 measurements from 4 duplicates for particle count and the average of 3 measurements for mass loss. The % value at the bottom of each column is the coefficient of variation (100 x standard deviation/mean).

Particle Size (µm)	**20 cycles**	**40 cycles**	**80 cycles**	**160 cycles**
0.08	158 834	155 936	162 090	158 497
0.12	136 799	134 039	142 913	137 335
0.16	81 114	86 256	90 028	85 164
0.2	56 935	61 163	69 402	63 149
0.24	32 815	39 882	42 701	39 465
0.28	16 874	23 623	25 510	22 115
0.32	8 894	12 646	14 551	14 075
0.36	3 752	6 214	7 961	7 425
0.4	2 660	4 606	4 725	4 725
0.44	1 787	2 501	2 521	2 918
0.48	516	1 271	1 886	1 886
0.52	258	933	854	1 112
0.56	179	655	556	635
0.6	60	397	496	318
> 0.6	179	775	557	617
Total surface particles ($1/mm^2$)	501 656 ±12.9%	530 897 ±15.2%	566 751 ±15.0%	539 436 ±22.2%
Mass loss (%)	0.6± 0.05	1.5± 0.15	2.1± 0.35	4.3 ± 0.85

3.5. Comparison of Surface Release Particles and Mass Losses of Nanocoating and Nanopaint Abraded under Dry and Wet Conditions

Table 8 provides a comparison of the total surface release particles and mass losses of NC and NP abraded under dry and wet conditions. The mass losses and total surface release particles for 160 abrasion cycles are included in this summary table. It can be seen in Table 8 (these data were also plotted in Figure 33a for clarity) that, total surface release particle counts for NC were almost the same (within experimental uncertainties, t-test, $p = 0.10$, not different in 95% confident level) under the same abrasion conditions at wet and dry conditions. However, NP generated significant more particles (t-test, $p = 0.019$, 99.1% significantly different) under the dry condition then the wet condition. Furthermore, NP generated many more surface release particles (with 10x higher amount) than NC under the same abrasion conditions.

Table 8. Comparison of total surface release particle count and mass losses of NC and NP abraded under dry and wet conditions; abrasion at 6.28 rad/s (60 rpm), 160 cycles, and 1000 g applied force

	Total Surface Particle Counts (per 1 mm^2) Dry	Total Surface Particle Counts (per 1 mm^2) Wet	Mass Loss (%) Dry	Mass Loss (%) Wet
NC	52 486 ± 14 %	64 346 ± 27.7 %	3.6 ± 0.1	6.4 ± 0.5
NP	696 207 ± 16.6 %	539 436 ± 22.2 %	4.2 ± 0.2	4.3 ± 0.85

For mass loss data (Figure 33b): wet abrasion produced more mass loss than those abraded under dry condition for NC. On the other hand, there was essentially no difference in mass loss between dry and wet abrasions for NP. Note that the mass loss measured at dry abrasion condition was performed by weighing the sample before and after abrasion (see Section 2.4) and the mass loss was much smaller than the mass of samples. For example, the sample (NC-on-wood substrate) weighed about 24 106 mg, and the mass of the wood substrate is 22 381 mg without NC. So the estimated mass of NC was about 1724 mg (± 10 %), which was almost 400 times heavier than the mass loss (≈ 62 mg). The error involved in measuring small mass changes in a heavy sample is large; therefore the results are less accurate. On the other hand, the mass loss obtained at wet abrasion condition was completed by weighing the resulting residues dried from the abraded liquids. The mass loss data at wet condition were more reliable

than the dry ones. To investigate the mass loss for NC and NP at different number of abrasion cycles, the mass loss as a function of cycles for (a) NC and (b) NP abraded in wet and dry conditions are plotted in Figure 34. The mass losses during both wet and dry abrasions were essentially a linear function of abrasion cycles, as shown in Figure 34. For the more rigid NC, the rate of mass loss by wet abrasion was greater than that by dry abrasion; the difference became larger as abrasion cycle increased. However, the rate of mass loss under dry and wet abrasions for softer, elastomeric NP was essentially the same.

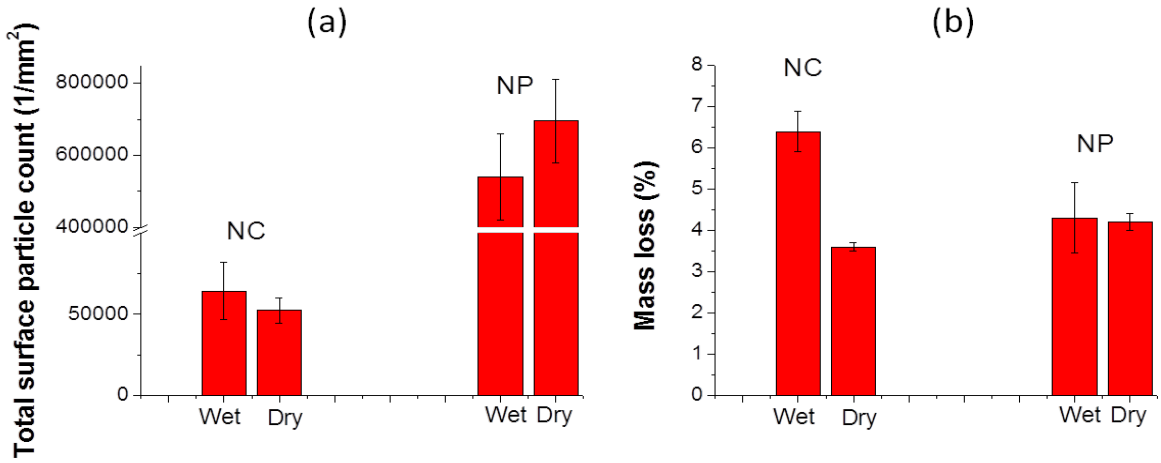

Figure 33. Comparison of (a) total surface particle counts (b) mass loss of NC and NP abraded under dry and wet conditions; abrasion at 6.28 rad/s (60 rpm), 160 cycles, and 1000 g applied force. The results are the average of 8 measurements for (a) particle count and the average of 3 measurements for (b) mass loss, and the error bars represent one standard deviation.

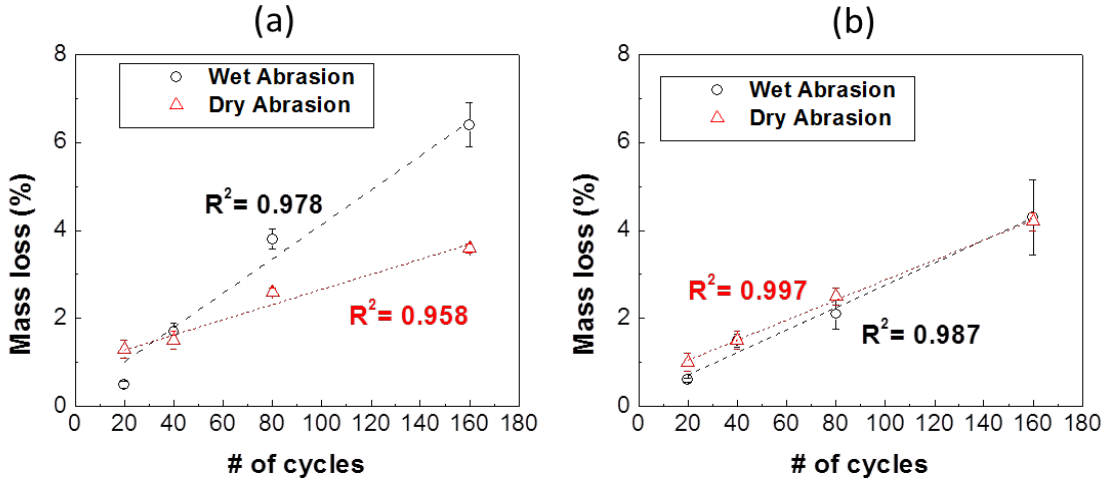

Figure 34. Mass losses of (a) NC and (b) NP as a function of number of cycles for wet and dry abrasions. All abrasions were performed using the MW2 wheel at 6.28 rad/s (60 rpm), 1000g applied force; each data point was the average of three specimens and the error bars represent one standard deviation. The dashed lines are the linear fit of each set of data.

3.5. Characterization of Released Particles in Water

To determine whether any nanoparticles were released from the NC and NP during abrasion in water, the release particles suspended in water were analyzed using the ICP-OES method. As indicated in the experimental section, in addition to the suspended release particles, a variety of "controlled" samples were studied, and the concentrations of three main elements (Al, Si, and Ti) in these "*controlled*" samples are presented in Table 9. Sample designations A to F are described in the experimental section and at the bottom of the table. Judging from the error values, the water "controlled" samples measured on the distilled water in the absence or presence of the accessory (A and B), wood, unabraded NC and NP, or wheel contained a very small concentration (< 1.5 μg) of Si.

Table 9. Concentrations of Al, Ti, and Si in controlled samples. The error represents one standard deviation based on 3 measurements from 3 duplicates

Sample	Al (μg)	Ti (μg)	Si (μg)
A	0.0099 ± 0.0029	ND*	0.66 ± 0.21
B	0.020 ± 0.013	ND*	0.831 ± 0.066
C	0.063 ± 0.016	0.00363 ± 0.0014	1.09 ± 0.10
D	0.0207 ± 0.0096	ND*	1.51 ± 0.15
E	0.031 ± 0.025	ND*	1.16 ± 0.67
F	0.106 ± 0.016	0.0056 ± 0.0026	1.04 ± 0.22

A. Distilled water alone
B. Water + liquid abrasion accessory (water placed in the accessory for 5 minutes, which is the time required to complete 160 cycles)
C. Water + wood + accessory (water placed in the accessory containing the wood disc for 5 minutes).
D. Water + nanocoated wood + accessory (water placed in the accessory containing the nanocoated wood disc for 5 minutes).
E. Water + wheel (MW2) (water having wheel immersed for 5 minutes).
F. Water + nanopaint + accessory (water placed in the accessory containing the nanopainted wood disc for 5 minutes).

*ND: not detected

Concentrations of the same three elements (i.e., Al, Si, and Ti) in water containing suspended release particles are summarized in Table 10. Sample designations are given at the bottom of the table. It should be mentioned that the upper part (u) (i.e., supernatant) and the lower part (l) (i.e., precipitate) were decanted approximately 5 h after the sonication, which was adequate for suspended particles to reach an equilibrium according to the time-dependent sonication study[30]. For NC, there is little evidence of Ti in the released particles in water for all cycles, and the concentrations of Al in the lower part are noticeable but did not follow any particular trend with respect to abrasion cycle. On the other hand, the amounts of Si in both the upper and lower parts of water containing NC release particles obtained at different abrasion cycles were substantial. Further, the concentrations of Si in the lower part, which clearly increased with increasing abrasion cycles, were higher than those in the upper part. The concentrations of Si in both the upper and lower parts of the sample are far exceeded those obtained from the various controlled samples (Table 9). The results indicate that the water suspended particles released from the NC contained a substantial amount of Si based materials. This is consistent with the EDXS results of the TGA residue (Figure 13), but somewhat inconsistent with the EDXS spectrum taken from the NC cross section (Figure 16), which showed the concentration of Al is much higher than that of Si.

For NP, the concentrations of all three elements in both the upper and lower parts collected at 160 cycles were sizable (Table 10). Further, the concentrations of these elements in the lower part were substantially greater than those of the upper part, suggesting a greater amount of material contained these three elements stayed at the bottom of the bottle sample than in the upper part after sonication for 5 h.

Table 10: Concentrations of Al, Ti, and Si in the samples containing suspended release particles from abraded experiments. The error represents one standard deviation based on 3 measurements (3 duplicates)

Sample	Al (μg)	Ti (μg)	Si (μg)
NC20 (u)	0.081 ± 0.003	0.004 ± 0.001	3.38 ± 0.13
NC20 (l)	0.601 ± 0.011	0.094 ± 0.007	6.72 ± 0.13
NC40 (u)	0.110 ± 0.005	0.002 ± 0.001	6.06 ± 0.17
NC40 (l)	1.056 ± 0.008	0.059 ± 0.005	11.15 ± 0.22
NC80 (u)	0.139 ± 0.004	0.002 ± 0.003	5.92 ± 0.28
NC80 (l)	2.328 ± 0.013	0.041 ± 0.008	22.51 ± 0.62
NC160 (u)	0.075 ± 0.007	0.016 ± 0.006	10.66 ± 0.46
NC160 (l)	0.747 ± 0.006	0.092 ± 0.004	27.21 ± 0.99
NP160 (u)	73.15 ± 0.89	9.09 ± 0.25	219 ± 17
NP160 (l)	2 932 ± 32	622.56 ± 0.31	1 264 ± 67

NC: nanocoating; NP: nanopaint; 20,40, 80, 160: number of cycles; l (lower): water and particles from the bottom part (Part B) of the liquid sample, u (upper): particles in the upper part (Part A) of the liquid sample; for s schematic of Part A and Part B, see experimental section. The error represents one standard deviation

4. Limitations

Nanoparticles release induced by abrasion process using a rotary abrader does not exactly mimic the real-world use of a commercial flooring nanocoating, such as walking with shoes, movements of furniture, scratching, and mopping. However, this method has been often utilized for wear resistance analyzes and recently used for generating particles for nanoparticle release study from polymer nanocomposites due to mechanical forces. This method presents a worst case scenario of wear. With controlled abrasion parameters and test procedures, this method can provide useful information/data for understanding the particle release mechanism and collect enough released particles for determining the quantities and properties of released nanoparticles.

The main purpose of the study is to investigate the test methods and protocols to quantify the generation of nanoparticles from a commercial flooring nanocoating and an interior nanopaint due to abrasion. The number and size distribution of particles that remained on the sample surface after abrasion both in dry and wet conditions were quantified using a LSCM microscopic/image analysis method. LSCM has its detection limit, and therefore cannot actually measure nanoparticles having particle sizes less than 80 nm. The LSCM microscopic/image analysis method is still useful for detecting release particles on the abraded surface, because most of the particles measured were nanoparticle clusters or nanoparticles embedded in polymer matrix.

In addition to limitations in the particle size measurements, the LSCM measurements reported here were only taken from eight different locations in the center of the abrasion ring for each sample. Therefore, the total numbers of released particles reported here does not reflect all particles being generated and released during this abrasion process. Released particles that were not captured may include:

1. particles on the all horizontal surfaces of the samples including the edges and outside the abrasion ring,
2. particles on the abrader wheel surface,
3. airborne particles [31], which may be emitted into the air.

Although, the number of particles presented here may not account for all the particles generated during the abrasion; this method is essential for the assessment of particle released

purpose for physical, chemical characterization, and toxicity studies, and this result can eventually lead to establish a correlation between the abrasion test method and real-world use.

5. Summary of Findings

Commercial polyurethane flooring coating (NC) and interior latex paint (NP) containing unknown amount of nanoparticles have been abraded with a Taber rotary abraser in air (dry abrasion) and in water (wet abrasion) to support the development of testing and measurement protocols for determining the quantities and properties of released nanoparticles. In Year 1 research, it was found that the commercial wheels, which are commonly specified in international standards for testing abrasion and wear resistance of coatings and paints, are not suitable for studies of abrasion-induced particle release from polymer nanocomposites because these wheels release their own particles during abrasion. The particles released from the wheels cannot be separated from those released from the test sample, and therefore conclusions regarding the particle release from the NC or NP cannot be made. One important task of the Year 2 research was to investigate a series of metallic wheels that have particular surface profiles suitable for abrading NC and NP without releasing their own particles. These specific wheels were designed and fabricated at NIST. Using these NIST-developed metallic wheels, abrasion of the commercial NC and NP under dry and wet (in water) conditions were carried out.

Based on the results of Year 1 research, only the number of abrasion cycles was varied, but other abrasion parameters, such as speed and applied force, were kept constant. In Year 2 tests, the most severe abrasion conditions (expected to generate the most particles) were selected: applied force =1000 g and speed = 6.26 rad/s (60 rpm). The number and size distribution of released particles that remained on the surfaces after abrasion (i.e., surface release particles), in air and in water were measured with the LSCM/image analysis method developed in Year 1. Further, during Year 2, the sample mass losses resulting from abrasion in both air and water were measured and compared, and the chemical composition of water containing release particles after abrasion was analyzed. A number of material properties that are relevant to their abrasion behaviors, such as mechanical properties before and after immersion in water, water uptakes in the films, inorganic content and their chemical composition, were also characterized. The main findings of Year 2 Research are summarized below:

1. Deep cross-patch or sandblasted noncorrosive stainless steel (e.g., 316 SS) metallic wheels (such as MW2 or MW4 shown in Figure 4) having a root mean square surface roughness between 5 μm and 7 μm were found suitable for reproducibly abrading in water and in air for flooring coatings and interior paints containing nanoparticles using a commercial rotary abraser. These metallic wheels at abrasion cycles that are manageable for testing (for example: 100 cycles) can generate a large number of release particles that can be used for physical, chemical characterization, and toxicity studies.
2. A substantial amount of released particles were detected on the surface after abrasion of NC and NP in both water and in air. The sizes of surface release particles of both nanoproducts abraded in air and in water varied between 0.08 μm and 0.6 μm, with (95 ± 1) % of them observed in the 0.08 μm to 0.3 μm range. The number of surface release particles decreased with increasing size.
3. The number of abrasion cycles has a little effect on the total surface release particles by dry and wet abrasion of both NC and NP, but has a strong effect on mass loss. The mass loss of both nanoproducts was nearly a linear function of abrasion cycle in both dry and wet conditions.
4. The mass loss of NC and NP was similar during dry abrasion (nearly 4 % at 160 cycles), but the mass loss of the NC was greater than that of the NP during wet abrasion. No apparent difference in mass loss between dry and wet abrasion was observed for NP, but the mass loss of the NC abraded in water was substantially higher than that abraded in air (3.6 % in air vs. 6.4 % in water). It was noted that NP took up almost 57 % water while NC absorbed just about one fifth of that amount. Further, the modulus value of water-saturated NC was only approximately one quarter of that when dry.
5. The total number of surface release particles of the softer elastomeric NP during abrasion in air and in water was approximately one order magnitude higher than that of the more rigid NC ($\approx 6 \times 10^5$ mm^{-2} for NP vs. $\approx 6 \times 10^4$ mm^{-2} for NC at 160 cycles).
6. For NC, a substantial amount of Si was detected in the supernatant and precipitate of water containing suspended release particles. The quantities in the precipitate were significantly higher than those in the supernatant and the amount of Si increased with increasing abrasion cycles, suggesting that the release particles during wet abrasion

contained Si based particles.

7. For NP, a high concentration of Al, Ti, and Si was observed in the supernatant and precipitate of water containing suspended release particles. The concentrations in the precipitate were markedly higher than those in the supernatant, suggesting that the release particles from NP during wet abrasion comprised many particles containing Al, Si, and Ti.

8. A protocol based on the information contained in this report can be used to assess (test) the relative potential release of particles from different NC and NP abraded in liquid or in air using the commercial rotary Taber abraser with NIST modified metallic wheels.

ACKNOWLEDGMENTS

The authors gratefully acknowledge project funding provided by the Consumer Products Safety Commission (CPSC) and valuable suggestions and comments by Dr. Treye Thomas of CPSC, as well as the assistances of the following NIST staff for various measurements: Drs. Lee Yu and Savelas Rabb for ICP-OES, Dr. Thomas Lam and Mr. Paul Stutzman for SEM and EDXS measurements, Mr. Eric Byrd, Mr. John Hettenhouser, and Miss Deborah Stanley for abrasion instrumentation and specimen fabrication.

REFERENCES

1. T. McNally and P. Pötschke, Eds., Polymer-carbon nanotube composites, preparation, properties, and applications, Woodhead Publishing, Philadelphia, 2011.
2. J. R. Potts, D. R. Dreyer, C. W. Bielawski, R. S. Ruoff, Graphene-based polymer nanocomposites, Polymer, 52 (2011) 5-25.
3. B. Li and W.H. Zhong, Review on polymer/graphite nanoplatelet nanocomposites, J. Mat. Sci., 46 (2011) 5595-5614.
4. S. Pavlidou and C.D. Papaspyrides, A review on polymer-layered silicate nanocomposites, Progress in Polymer Science, 33 (2008) 1119-1198.
5. H. Zou, S.S. Wu, and J. Shen, Polymer/silica nanocomposites: preparation, characterization, properties, and applications, Chemical Reviews, 108 (2008)3 893-3957.
6. R. McIntire, Common nano-materials and their uses in real world applications, Science Progress, Vol. 95, no. 1.
7. Nanotechnology market forecast to 2013, Report by ResearchandMarkets, http://www. researchandmarkets.com/research/2012b4/nanotechnology_mar
8. Nanomaterials in plastics and advanced polymers, Market Report # 52, April, 2012, Future Markets, Inc.
9. A.D. Maynard, Nanotechnology: Assessing the risks, Nanotoday, 2: 22-33 (2006).
10. A. Nel, T. Xia, L. Mädler, N. Li, Toxic Potential of Materials at the Nanolevel, *Science*, 311, 622-627 (2006).
11. C. Poland, R. Duffin, I. Kinloch, A. Maynard, W. A.H. Wallace, A. Seaton, V. Stone, S. Brown, W. MacNee, K. Donaldson, Carbon nanotubes introduced into the abdominal cavity of mice show asbestos-like pathogenicity in a pilot study, Nature Nanotechnology, 3 (2008) 423-428.
12. K. Aschberger, H. Johnson, V. Stone, R. Aitken, S. Hankin, S. Peters, C. Tran and F. Christensen, Review of carbon nanotubes toxicity and exposure – Appraisal of human health risk assessment based on open literature, Critical Reviews in Toxicology, 40(9) (2010): 759-790.

13. R. D. Handy, T.B. Henry, T.M. Scown, B.D. Johnston, C.R. Tyler, Manufactured Nanoparticles: Their Uptake and Effects on Fish-A Mechanistic Analysis, Ecotoxicology 17 (2008) 396–409.
14. L.K. Adams, D.Y.Lyon, P.J.J. Alvarez, Comparative Ecotoxicity of Nanoscale TiO2, SiO2, and ZnO Water Suspensions, Water. Res. 40 (2006), 3527–3532.
15. J. Lee, S. Mahendra, P. J. J. Alvarez, Nanomaterials in the Construction Industry: A Review of Their Applications and Environmental Health and Safety Considerations, ACSNano, 4 (2010) 3580-3589.
16. A. R. Köhler, C. Som, A. Helland̲a, and F. Gottschalk, Studying the potential release of carbon nanotubes throughout the application life cycle, J. Cleaner Prod., 16 (2008) 927-937.
17. B. Nowack, et al., Potential scenarios for nanomaterial release and subsequent alteration in the environment, Env. Toxicol. Chem., 31 (2012) 50-59.
18. B. Nowack, et al., Potential release scenarios for carbon nanotubes used in composites, Environmental International, 59 (2013) 1-11.
19. W. Wohlleben, et al., On the life cycle of nanocomposites: comparing released fragments and their in-vitro hazards from three release mechanims and four nanocomposites, Small, 7 (2011) 2384–2395.
20. http://www.researchandmarkets.com/reportinfo.asp?report_id=1824738&t=t
21. L. Schlagenhauf, T.T. Bryan, B. Chu, J. Buha, F. Nüesch, and J. Wang, Release of carbon nanotubes from an epoxy-based nanocomposite during an abrasion process, *Environ. Sci. Technol.*, published, Jun 2012.
22. D. Bello, et. al., Exposure to nanoscale particles and fibers during machining of hybrid advanced composites containing carbon nanotubes. J. Nanopart. Res., 2009, 11, 231-249.
23. D. Gohler, M. Stintz, L. Hillemann, and M. Vorbau, Characterization of nanoparticle release from surface coatings by the simulation of a sanding process. Ann. Occup. Hyg., 54 (2010) 615-624**.**
24. M. Vorbau, L. Hillemann, L. and M. Stintz, Method for the characterization of the abrasion induced nanoparticle release into air from surface coatings, J. Aerosol Sci., 40 (2009) 209-217.
25. L. Golanski, A. Gaborieau, A. Guiot, G. Uzu, J. Chatenet, and F. Tardif, Characterization of abrasion-induced nanoparticle release from paints into liquids, J. Phys. Conf. Ser. 304 (2011)

012062.

26. L. Reijnders, The release of TiO_2 and SiO_2 nanoparticles from nanocompoites, Polymer Degradation and Stabilization,94 (2009) 873-876.
27. S. Sachse, et al., The effect of nanoclay on dust generation during drilling of PA6 nanocomposites, J. Nanomaterials, 2012, DOI10.151155/2012/189386.
28. M. Busquets-Fite, E. Fernandez, G. Janer, G. Vilar, S. Vazquez-Campos, R. Zanasca, C. Citterio, L. Mercante, V. Puntes. Exploring release and recovery of nanomaterials from commercial polymeric nanocomposites. Journal of Physics: Conference Series 429:012048, 2013.
29. D. Göhler, A. Nogowski, P. Fiala, M. Stintz. Nanoparticle release from nanocomposites due to mechanical treatment at two stages of the life-cycle. Journal of Physics: Conference Series 429:012045, 2013.
30. T. Nguyen, L. Sung, J. Chin, A. Persily. Characterization of Airborne Nanoparticle Released from Consumer Products, Final Report to U.S. Consumer Product Safety Commission Interagency Agreement CPSC-I-12-0007, TN 1787, April 2013.
31. AK. Persily, J. Lo, S. Nabinger, D. Poppendieck, L. Sung. Characterization of Airborne Nanoparticle Released from Consumer Products, NIST report 2014.
32. LP. Sung, J. Jasmin J, X. Gu, T. Nguyen, JW Martin. Use of Laser Scanning Confocal Microscopy for Characterizing Changes in Film Thickness and Local Surface Morphology of UV Exposed Polymer Coatings. J. Coat. Technol. Res. 2004; 1: 267-276
33. The NIH freeware *ImageJ* developed by National Institutes of Health (NIH) can be downloaded from http://rsb.info.nih.gov/ij/.
34. J. K. Lancaster. Abrasive Wear Of Polymers, Wear, 14 (1969) 223-239.
35. E.J. Petersen, T. Lam, J.M. Gorham, K.C Scott, C.J. Long, D. Stanley, R. Sharma, J.A. Liddle, B. Pellegrin and T. Nguyen. Methods to assess the impact of UV irradiation on the surface chemistry and structure of multiwall carbon nanotube epoxy nanocomposites, Carbon, Available online 11 December 2013, ISSN 0008-6223, DOI:10.1016/j.carbon.2013.12.016.
36. J. Comyn. Polymer Permeability Elsevier Applied Science, London, 1985.